Representation of symmetry in the extrastriate visual cortex from temporal integration of parts: An EEG/ERP study

Giulia Rampone [a,*], Alexis D.J. Makin [a], Semir Tatlidil [b], Marco Bertamini [a]

[a] University of Liverpool, UK
[b] Brown University, USA

ABSTRACT

When symmetry is present in the retinal image, a symmetry-sensitive network in the extrastriate visual areas activates, and response magnitude scales with degree of regularity. Is this activation driven by the regularity in the image, or can the network recover regularity of an object? We investigated whether the network responds to bilateral symmetry for dynamically occluded shapes, and thus responds to symmetry in the object. The stimulus was an irregular shape partly occluded by a rectangle. After 500 ms, the rectangle was displaced to the other side, occluding the previously visible half, and revealing the other half for 1000 ms. Therefore, no symmetry was present in the image at any point in time. Exp.1 and Exp.2 used vertical and horizontal axis of reflection, and in Exp. 3 there was no occluder. Participants could detect symmetry with >80% accuracy. More importantly, ERP analysis showed a symmetry-specific response from ~300 ms after presentation of the second half of the shape. When integration was made from halves of asymmetric whole shapes (Exp.4), and when symmetry was not task-relevant (Exp.5), no symmetry response was recorded. The results show, for the first time, an electrophysiological evidence of symmetry representation in the brain obtained by assembling information over time into a unitary gestalt. The integration process occurs when observers look for symmetric matches between the parts, and only if these are perceived as belonging to the same object.

1. Introduction

Shape perception relies on patterns of information projected onto the retina. However, the visual system has the remarkable ability of constructing coherent shape representations from scattered, distorted and partially occluded images. The reconstruction of shape often happens over both space and time. For example, an observer can recognise an object moving behind an occluder even though the motion hides some parts of the object as it reveals others.

Symmetry is a ubiquitous shape property that characterises many natural and man-made objects. To see symmetry, the visual system must find non-accidental spatial relationships between elements and group them together to form a visual whole (Jenkins, 1983; Wagemans et al., 1991; Wagemans et al., 1993). We also know that processing of symmetry happens efficiently even with brief presentations (Barlow and Reeves, 1979; Carmody et al., 1977; Julesz, 1971) and with peripheral presentations (Barlow and Reeves, 1979; Julesz, 1971; Rampone et al., 2016; Saarinen, 1988; Wright et al., 2017). It is robust to transformations such as skewing and perspective slant (Makin et al., 2015; Sawada and

Pizlo, 2008; Wagemans et al., 1991).

Neuroimaging research has discovered a network of symmetry-sensitive areas in the extrastriate visual cortex (Bertamini and Makin, 2014; Bertamini et al., 2018; Bona et al., 2014; Chen et al., 2007; Kohler et al., 2016; Martinovic et al., 2018; Sasaki et al., 2005; Tyler et al., 2005; Wright et al., 2018). The response within this network scales with proportion of symmetry/noise (Palumbo et al., 2015; Sasaki et al., 2005) and with *perceptual saliency* of the regularity in the image (Makin et al., 2016). However, images generated by the natural environment rarely contain perfect symmetry. Rather, the representation of *object symmetry* often extracted from broken or distorted *retinal image symmetry* (i.e. slanted surfaces, edges that are below threshold, or occlusion by other objects). Any efficient symmetry-detection mechanism must overcome noise and occlusion.

This study uses electroencephalography (EEG) to test whether extrastriate brain areas can achieve a representation of reflectional symmetry through integration of temporally separated parts. Our analysis of event related potentials (ERP) from five experiments shows that representation of object symmetry is similar to that evoked by retinal

---

image symmetry. However, this process does not happen automatically and requires active discrimination of symmetry in the stimulus.

1.1. Neuroscience of symmetry perception

The neural basis of symmetry perception has been investigated for more than a decade (see reviews Bertamini and Makin, 2014; Bertamini et al., 2018; Cattaneo, 2017; Treder, 2010). There is a network of symmetry-sensitive regions spanning V3, V4 and the object sensitive Lateral Occipital Cortex (LOC). Conversely, early visual areas V1 and V2 and dorsal stream areas MT and IPSO are not sensitive to symmetry (Chen et al., 2007; Keefe et al., 2018; Kohler et al., 2016; Sasaki et al., 2005; Tyler et al., 2005). Meanwhile, Transcranial Magnetic Stimulation (TMS) studies have shown that LOC plays a causal role in symmetry perception (Bona et al., 2016; Bona et al., 2014; Cattaneo et al., 2014).

Event Related Potential (ERP) studies have consistently found negative amplitude at posterior electrodes when participants view symmetrical configurations (Höfel and Jacobsen, 2007; Makin et al., 2016, 2015; Makin et al., 2012a,b; 2014; Norcia et al., 2002; Palumbo et al., 2015; Rampone et al., 2014; Wright et al., 2017). This ERP component has been called Sustained Posterior Negativity (SPN, Fig. 1A and B). The SPN is a relative measure, given by the difference between symmetry and asymmetry waves (Fig. 1B shows the SPN as a difference wave). The SPN is recorded over posterior electrodes (like PO7 and PO8 in Fig. 1C) and it is likely to be generated by the extrastriate symmetry network (Kohler et al., 2016; Kohler et al., 2018; Makin et al., 2012a,b; Sasaki et al., 2005). The SPN is generated whether attention is directed to symmetry or to other aspects of the display (Höfel and Jacobsen, 2007; Jacobsen and Höfel, 2003; Kohler et al., 2016; Makin et al., 2013, 2014; Norcia et al., 2002; Rampone et al., 2014; Wright et al., 2017). Therefore, we describe the SPN as *automatic* (as long as symmetry is available in the image). Moreover, the SPN is not specific to bilateral symmetry but scales with the saliency or perceptual goodness of different regularities, including rotational symmetry and Glass patterns (Makin et al., 2016, 2013).

Theoretical models suggest symmetry detection involves finding correlation across spatial locations. One hypothesis is that the brain may

be sensitive to representations of holographic regularities and respond parametrically to these when they are in the image (holographic model, van der Helm and Leeuwenberg, 1996). Alternatively, process models suggest that symmetry detection depends on first-order regularities (i.e. virtual line segments connecting the dots belonging together in a symmetric pair; see Jenkins, 1983) and second-order regularities (i.e. two pairs of symmetric pairs define virtual quadrangles; see Wagemans et al., 1991, 1993), which are bootstrapped along the local axis of symmetry. Brain response to symmetry may otherwise depend on output from spatially oriented filters, yielding to a number of blobs which are aligned along a putative axis of symmetry (Cohen and Zaidi, 2010; Dakin and Hess, 1997; Dakin and Watt, 1994; Osorio, 1996; Poirier and Wilson, 2010; Rainville and Kingdom, 2000; Scognamillo et al., 2003). Poirier and Wilson (2010) proposed a comprehensive spatial filtering model, in which shape symmetry is recovered through five stages, starting from the detection of the shape outline using small-scale oriented filter, to quantification of the amount of pairs of curvatures at opposite angular distances from an object-centred putative symmetry axis. This model applies to a wide range of symmetries, including faces, making it a biologically valid model. The key difference across all these models is that they rely either on precise or more crude correlations between stimulus elements (for an exhaustive review of the models of symmetry processing see (Treder, 2010; van der Helm, 2014).

There are neurophysiological evidences in support to these models. Palumbo et al. (2015) observed that amplitude of SPN scales linearly with proportion of regularity in the image (Fig. 1D), whilst Makin et al. (2016) observed strong correlation between the estimated strength of symmetry percept (as predicted by the *holographic model*; van der Helm and Leeuwenberg, 1996) and its neural signal. These findings suggest that brain responses to symmetry reflect a perceptual coding of non-accidental spatial regularities in the image.

1.2. Study rationale, aims and hypothesis

The extrastriate symmetry network is sensitive to symmetry in the image. However, in the real world, image symmetry is often degraded by different levels of noise, low contrast, illumination changes, perspective
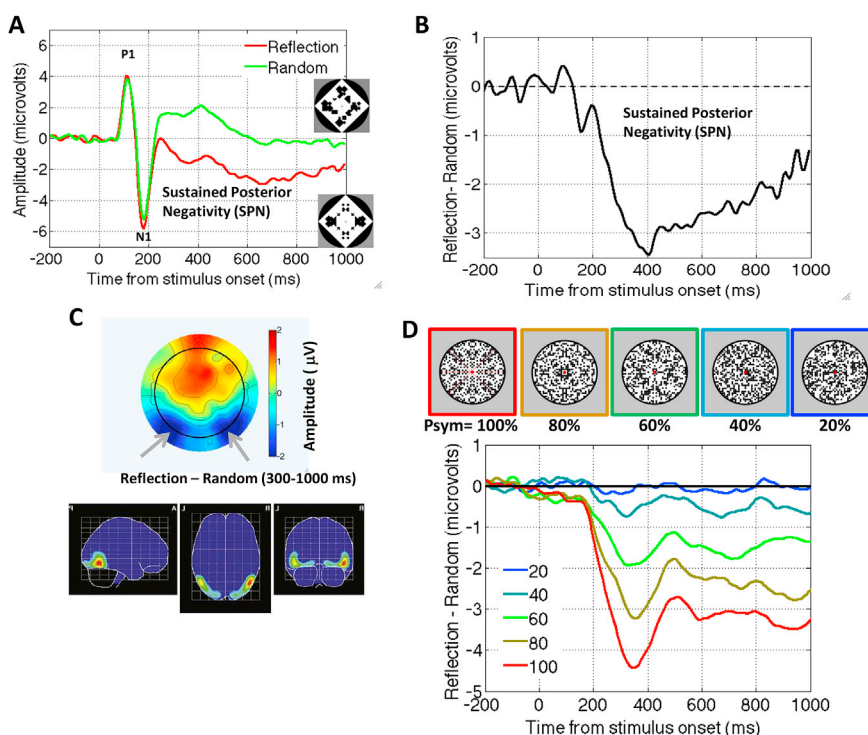

Fig. 1. The Sustained Posterior Negativity (SPN). (A) Grand average waveforms from PO7/PO8 electrodes in symmetry and random (asymmetry) conditions. Example stimuli are shown in insets. (B) Grand average SPN shown as a difference wave (symmetry – random). (C) Topographic difference map from 300 to 1000 ms post stimulus onset (SPN is coded as blue at posterior electrodes) and estimated cortical sources of the grand average SPN.
Data from Experiment 1 of Makin et al. (2012a,b). (D) Data from Palumbo et al. (2015) showing how the SPN scales with proportion of symmetry of the patterns (see Makin et al., 2016 for more examples of scaling).

and occlusion. In these situations, the visual system cannot rely on finding point-to-point spatial correspondences between elements (i.e. first- and second- order structures) for symmetry detection. An efficient system needs to engage in additional computations that can achieve a global representation of symmetry at the object-level.

Makin et al. (2015) showed that symmetry network can respond to symmetry presented in images with a 50 deg perspective slant. They used two-fold reflection symmetry patterns, presented either on the fronto-parallel (i.e. two axes on retina, two axes in the object) or slanted plane (i.e. one axis on retina, two axes in the object). The amplitude of the SPN was view invariant (i.e. the same for flat and slanted symmetry) if participants actively discriminated regularity, but it was reduced for slanted stimuli when they discriminated the colour of the dots. This study provided evidence of an ability of the symmetry-network to go beyond retinal information and achieve a representation of symmetry in the object (see also Keefe et al., 2018). However, it is possible that this perspective normalisation process draws on additional neural resources, and is engaged only when necessary (i.e. when symmetry is task-relevant). In conditions in which attention is directed to other stimulus features, no perspective normalisation occurs and the extrastriate symmetry network only respond to the information present in the retinal image.

Object representation can also go beyond the image by overcoming occlusion. For instance, there is a classic literature on amodal perception (Michotte et al., 1964). The visual system infers the occluded parts of visible objects. Such amodal completion is automatic (*seeing* rather than *thinking* in Kanizsa's words: Kanizsa and Gerbino, 1982) and fast (Bruno et al., 1997). The visual system can also construct holistic object representations by integration of stimulus fragments (Kourtzi and Kanwisher, 2001; Lerner et al., 2002; Rauschenberger et al., 2006). Within the LOC, there is a final representation of a complete object (Kourtzi and Kanwisher, 2001; Lerner et al., 2002), and the LOC can send feedback signal to lower-level areas to support the filling-in of missing information (O'Reilly et al., 2013; Rauschenberger et al., 2006; Wyatte et al., 2012).

In static configurations, this process relies on the retinotopic correspondences between the visible parts (O'Reilly et al., 2013). A challenge for the visual system is to receive and integrate partial information across the *temporal domain* as well as the *spatial domain*. Consider, for example, an occluder moving in front of an object and revealing parts of the object whilst covering others. In this case, the relationship between the visible parts is only revealed over time. To create a coherent representation of the object, the briefly viewed fragments must remain perceptually available for a short time after occlusion so that they can be integrated with later-appearing fragments (*Persistence hypothesis*, Palmer et al., 2006). The stimulus fragments need to be stored in a *sensory buffer,* at a non-retinotopic locus, where the information is not erased by new inputs to the same receptive fields (*non-retinotopic Sensory Memory*, Öğmen and Herzog, 2016). The *object-based* information stored in the sensory buffer can then be integrated with the new visual inputs (Scharnowski et al., 2007).

Considering what discussed so far, a timely research question is whether a global representation of symmetry in the extrastriate cortex can be constructed by integration of transient visible shape fragments with those already stored in the sensory buffer.

We designed a series of experiments, in which a novel, jagged abstract shape (a polygon with a texture of dots) was presented next to a vertical rectangle (t1). Therefore, a whole object was perceived as partly occluded by the rectangle. After a short interval, the occluder changed position to reveal the *hidden* part whilst covering the previously *visible* half (t2). In some trials, the two halves formed a mirror symmetric shape, and in the other trials the two halves were unrelated to each other (see Fig. 2A and B). In other words, the whole was sometimes symmetrical, and sometimes asymmetrical. We predicted that an SPN would be generated when the symmetrical whole is perceived.

There is behavioural evidence that the visual system can achieve global representations of symmetry through dynamic integrative
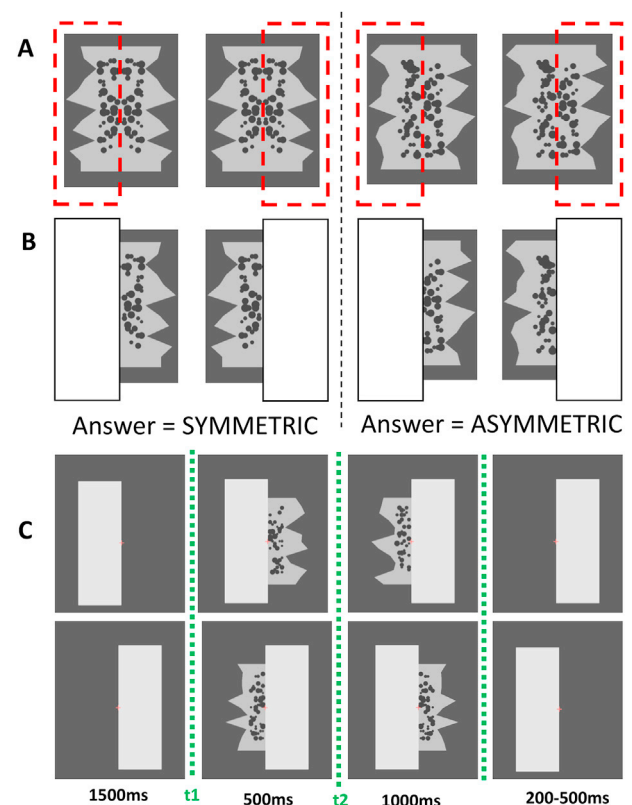

Fig. 2. (A) Example of the stimuli used in the experiment. Shapes were polygons with a dark-grey dots texture. Both shapes were formed by generation of two separate halves along one central vertical mid-line. The shapes on the left match to form bilateral symmetry; the shapes on the right do not match. The red dashed bar is provided for illustrational purposes and mimics the actual occluder bar presented in the experiment. Note that it is impossible to distinguish between symmetric and asymmetric from information in just one image: No single frame of the display ever contained symmetry. (B) Examples of the stimuli with the occluder. (C) The experimental procedure. After a baseline interval of 1500 ms, the stimulus shape is presented behind the occluder bar (t1). After 500 ms the bar shifts position and reveals the other half of the stimulus (t2), whilst covers the previously visible part. The stimulus disappears after 1000 ms. Occluder could shift either left → right (top) or right → left (bottom). All stimuli were generated afresh, and a new stimulus was presented on each trial. In this example, both shapes are symmetric.

processes. For example, symmetry detection improves with multiple consecutive presentations of symmetry patterns. This suggests that the visual system can engage in cumulative temporal integration processes that enhance the symmetry response (Niimi et al., 2005, 2008; Sharman and Gheorghiu, 2017, 2018; Sharman et al., 2018; Tyler et al., 1995). Of particular relevance for our study are the works of Niimi et al. (2005) and Sharman et al. (2018). Niimi et al. (2005) presented two asymmetric patterns in rapid succession, which led to detection of fused symmetry images if presented close enough in time. This was an example that visual system can perform a global, as opposed to local, processing of the spatial relationship between elements. However, it is important to note that, in Niimi et al. (2005), this global processing relied on mechanisms that integrate persistent retinal afterimages with non-overlapping upcoming information. In our study, an overlapping object (i.e. a bright occluder bar, Fig. 2B) masks the retinal image of previous information. Therefore, the information presented in t1 should remain available in a *non-retinotopic* sensory buffer in order to be integrated with information in t2 (Fig. 2B). Sharman et al. (2018) investigated whether symmetry mechanisms can integrate symmetrically matched halves of patterns presented
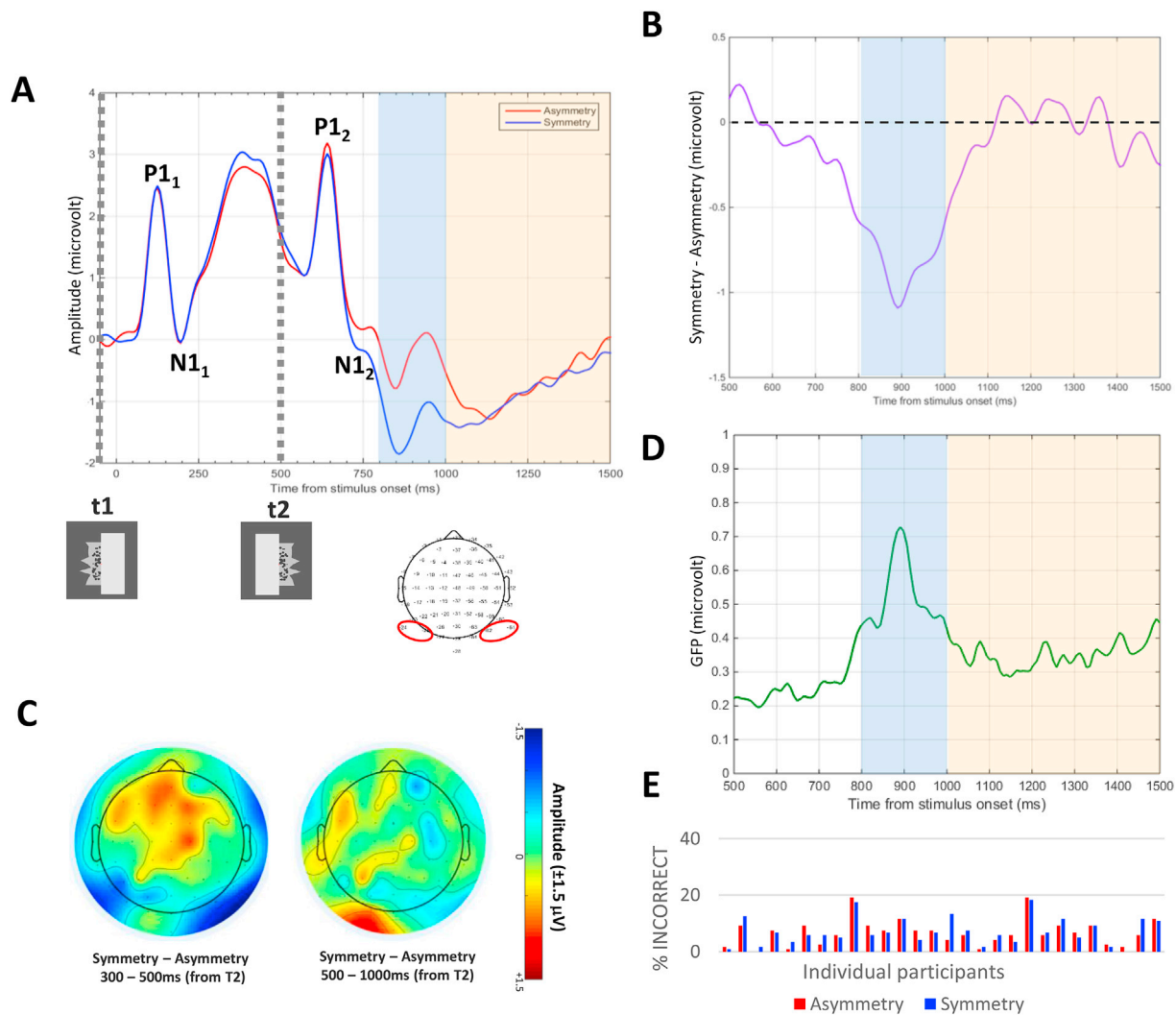
Fig. 3. *Experiment 1 Results* (A) Grand average ERPs averaged across electrodes P9 PO7 P10 PO8 (red ovals on inset). Time-window displayed is from the onset to the offset of the shape behind the occluder. From 0 (t₁) to 500 ms the first half is visible. At this point, the participant is not able to distinguish between symmetry and asymmetry. At 500 ms (t₂) the occluder shifts and reveals the other part of the shape. After this, the current visual information can integrated with the stored representation of the previously seen half shape, and a symmetry – asymmetry ERP is observed after ~300 ms. (B) Zoomed plot of the Grand average ERP shown as a difference wave (Symmetry – Asymmetry). The blue and orange regions indicate the time-windows used for the analysis. (C) Topographic difference maps (Symmetry – Asymmetry) from the time-window 300–500 ms and 500–1000 ms. (D) Global Field Power (GFP) plot showing standard deviation of amplitude across the 64 electrodes from t₂ to end of the epoch. (E) Individual participant's percentage of incorrect responses for both asymmetry and symmetry conditions. Note that these trials were not included in the ERP analysis.

with temporal delay. Each image contained half of a symmetrical pattern and half of a random noise pattern; images containing left and right halves of the symmetrical and noise patterns were alternated at given temporal frequencies. Participants could detect symmetry with temporal frequencies higher than approximately 17 Hz. This showed a cumulative temporal enhancement of the symmetry response even when symmetry parts were presented at different points in time.

Finding point-to-point spatial relationships in the retinal image seems not to be a necessary condition for symmetry detection. As the visual brain processes information in a dynamic and integrative manner, when it comes to general object representation, the same flexibility seems to apply to symmetry-responsive networks. This study aimed at investigating brain representations of symmetry when integration of transient (asymmetric) parts is required.

This study aimed at answering three fundamental questions. (i) First, would a symmetry-ERP response be generated when two separate (asymmetric) parts of a shape are viewed at different timepoints? Experiment 1 used a vertical axis of symmetry (Fig. 2). If symmetry information from the half-shape seen at t₁ persists in a perceptual buffer

until the second part appears at t₂, then the computation of spatial relatability can be performed to connect visible and occluded regions into a unified perceptual whole. Vertical orientation is special because it is more salient, and the pattern straddles the midline of the visual field (Bertamini et al., 1997; Friedenberg and Bertamini, 2000). In Experiment 2 stimuli had a horizontal axis (Fig. 4). The experiment aimed at replicating the findings observed in experiment 1 and confirming that integration happens independently of axis orientation.

(ii) Second, would the spatial relationship between parts be computed even if these were perceived as two independent and unrelated objects? Psychophysical findings have suggested that symmetry may be important for perception because it indexes objecthood (Baylis and Driver, 1995; Bertamini et al., 2002; Bertamini et al., 1997; Corballis and Roldan, 1974; Koning and Wagemans, 2009a; Makin et al., 2012a,b; Treder and van der Helm, 2007). Conversely, (perceived) objecthood might be a necessary condition for integration of parts into a symmetric whole. In the first two experiments, the presence of a rectangle creates the impression of a whole object partly hidden behind an occluder. In Experiment 3 there was no occluder (Fig. 6). We reasoned that without
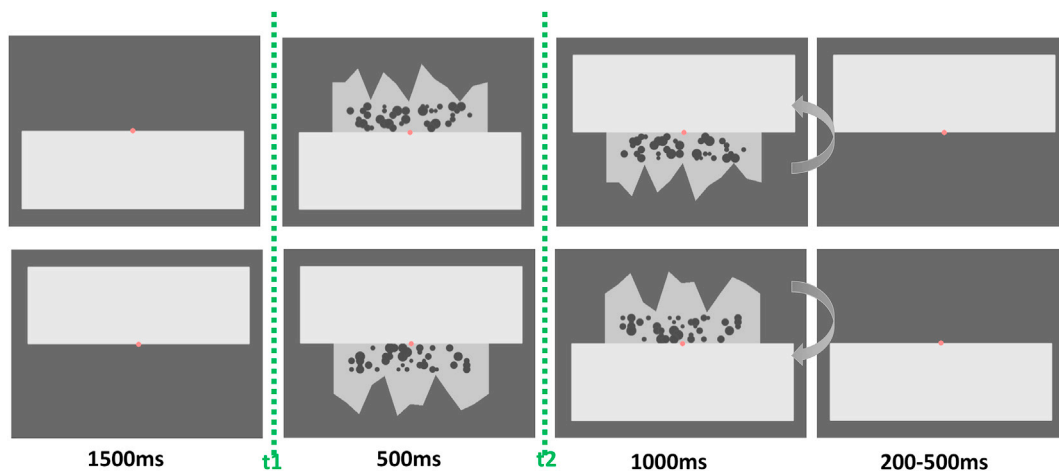
Fig. 4. Example of stimuli and experimental procedure in Experiment 2. The time sequence is shown from left to right. The stimuli were identical to Experiment 1, but rotated. The occluder moved down→up (top) or up→down (bottom). In the figure both shapes are symmetric.

the occluder, the half-shapes would be perceptually interpreted as independent objects. Experiment 4 further tested whether the two halves would be combined even if these were perceived as already parts of two independent and unrelated objects. Experiment 4 was identical to Experiment 1, except that the occluder was replaced by another randomly constructed half shape (forming a whole asymmetrical shape, see Fig. 10). This experiment tested whether fusion of currently visible parts into perceptual wholes interferes with the formation of extra-retinal representation of the integrated whole.

(iii) Third, does this temporal integration process happen automatically? Experiment 5, participants performed an oddball detection task on a symmetry-unrelated stimulus property (i.e. colour) (Fig. 11). We know that the symmetry-specific SPN component is generated automatically for fully visible symmetry during oddball detection (Makin et al., 2013). Conversely, in slanted displays (which require a normalisation process) attention must be focused on active symmetry-discrimination (Keefe et al., 2018; Makin et al., 2015). We thus expected that when attention was directed away from symmetry, no SPN response would be recorded, because a representation of symmetry would require an effortful integration process (and no symmetry was ever presented in the image).

To anticipate our results, we found that a representation of symmetry is formed in the symmetry-network in the presence of dynamic occlusion (Experiment 1, 2 and 3). This representation requires parts to be perceived as not belonging to different (asymmetrical) objects (Experiment 4). Finally, participants' attention must be directed towards symmetry for integration to happen (Experiment 5).

The General Method session, with a detailed outline of the variations among the different experiments is provided at the end of the paper for ease of reading.

2. Experiment 1 (vertical axis)

In this experiment shapes with a vertical reflection and asymmetric shapes were half-covered by a white rectangle. Therefore, only asymmetrical halves were visible on any given frame. After an interval of 500 ms, the occluder shifted position to reveal the unseen half the shape whilst covering the previously visible part. Participants discriminated whether the partially occluded shape was *symmetric* or *asymmetric*.

2.1. Results

2.1.1. Behavioural

The proportion of incorrect responses was: mean 6.8% (SE 0.9), median 6.25% (range 0–19) for asymmetry; mean 7.2% (SE 0.9), median 6.25% (0–18) for symmetry. Paired T-test for the symmetry – asymmetry

difference was performed on the log-transformed data. No significant difference between conditions was observed ($t(27) = -0.55$, $p = .6$). Fig. 3E reports the individual participant's percentage of incorrect responses in their original form. Note that ERPs analysis was performed only on trials where the correct decision was made.

Fig. 3A shows the Grand Average ERPs (electrodes P9 PO7; P10 PO8) for the whole epoch going from the onset of the first-half stimulus (t_1) to the offset of the second-half stimulus. The first 500 ms ($t_1 - t_2$) one half of the shape was shown whilst the other half was covered by the occluder. In this time-window the symmetry and asymmetry waves were nearly identical. They separated from around 300 ms into t_2 (time in which the second half is shown). This corresponds to the typical latency of the SPN (250 ms from stimulus onset, Fig. 1), although in this case, the negativity was not 'sustained', but terminated 500 ms into t_2. This is shown by the symmetry – asymmetry difference wave in Fig. 3B. Since no symmetry-related response was ever recorded before t_2, time-points in the analysis will always refer to *times from t_2.*

2.1.2. ERPs

We analysed ERPs within two time-windows: 300–500 ms and 500 to 1000 ms from t_2 (Fig. 3A–D). The factors in a $2 \times 2 \times 2$ repeated measure ANOVA were: Time-window (300–500 ms, 500–1000 ms), Hemisphere (left, right) and Regularity (symmetry, asymmetry). There was a main effect of Time-window ($F_{(1,27)} = 42.4$, $p < .001$, partial $\eta^2 = 0.63$) and a main effect of Regularity ($F_{(1,27)} = 13.6$, $p = .001$, partial $\eta^2 = 0.36$). Importantly there was a significant interaction between Time-window and Regularity ($F_{(1,27)} = 46.8$, $p < .001$, partial $\eta^2 = 0.63$). These effects resisted sequential Bonferroni corrections for the control of familywise error rate (FWER) (see Supplementary Material 1). Follow up tests of simple effects (Bonferroni adjusted) confirmed that mean symmetry – asymmetry difference was significant in the earlier 300–500 ms time-window ($M = -1.09$, $SE = 0.2$; $p < .001$), whilst there was no difference in the later time-window ($M = -0.21$, $SE = 0.2$; $p = .2$). No other main effects or interactions were observed ($Fs < 3.8$, $ps > .2$). These effects resisted sequential Bonferroni procedure for the control of familywise error rate (FWER) (see Supplementary Material 1).

The topographic maps in Fig. 3C confirm this result, showing posterior activity in the earlier time-window but not in the later one. Moreover, Global Field Power (GFP; the standard deviation of amplitudes across the 64 electrodes) peaked at 300 ms-500 ms Fig. 3D). This parallels the time-course of the posterior difference wave (Fig. 3B). Together the results suggested that integration of the parts happened 300 ms–500 ms after the appearance of the second half of the shape. This integration process generates a negativity over the posterior regions (where the SPN response to visible symmetry is typically recorded).

2.2. Discussion of experiment 1

On each trial, an irregular shape was presented next to a rectangle, creating the percept of a shape half-covered by an occluder. After for 500 ms (t_1), the occluder changed position. The other half-shape was revealed as either a reflection of the first or it was unrelated to it (t_2), as illustrated in Fig. 2. All participants could discriminate between symmetry vs. asymmetry with >80% accuracy. We analysed ERPs only from trials in which a correct discrimination was made. In the first interval, no difference in the ERP for symmetry vs asymmetry was observed. This was expected as no symmetry was present in the image and participants could not guess the identity of the shape from the information provided.

A response SPN like wave was recorded around 300 ms from the onset of the second image. This difference in amplitude between reflection and asymmetry may be attributable to the integration process of the two halves. If reflection is constructed, amplitude is more negative than when asymmetry is constructed. The latency and topography of this response corresponded to the SPN generated by image symmetry (Bertamini and Makin, 2014). However, this *posterior negativity* was not *sustained*. As shown in Fig. 3B, the difference wave terminated at 600 ms from t_2. Although SPN waves are usually longer than this, this early component often contains the largest effect (Makin et al., 2016; Wright et al., 2017).

3. Experiment 2 (horizontal axis)

This experiment (N = 28) was identical to Experiment 1, with the sole difference that stimuli were organised horizontally (see Fig. 4). Horizontal symmetry elicits similar SPN to vertical symmetry (Wright et al., 2015). However, the vertical axis is associated with better performance (Bertamini et al., 1997; Friedenberg and Bertamini, 2000), and it has been speculated that this is due to the projection of each half of the stimulus to one or the other hemisphere (*callosal hypothesis*; Herbert and Humphrey, 1996; Mach, 1886). It was indeed the case that in Experiment 1, with central fixation, corresponding halves were shown in the two hemifields. Moreover, hemispheric asymmetries in attention and spatial processing are well known (e.g. Baijal and Srinivasan, 2011; Papousek and Schulter, 2006; Shulman et al., 2010). Therefore, we decided to test the generality of the finding with a horizontal configuration.

3.1. Results

3.1.1. Behavioural

For the asymmetry condition mean percentage incorrect responses was 7.5 (SE 0.9), median was 6.6 (range 1–18); for the symmetry condition mean was 7 (SE 0.7) and median 5.8 (range 2.5–20). Paired T-test
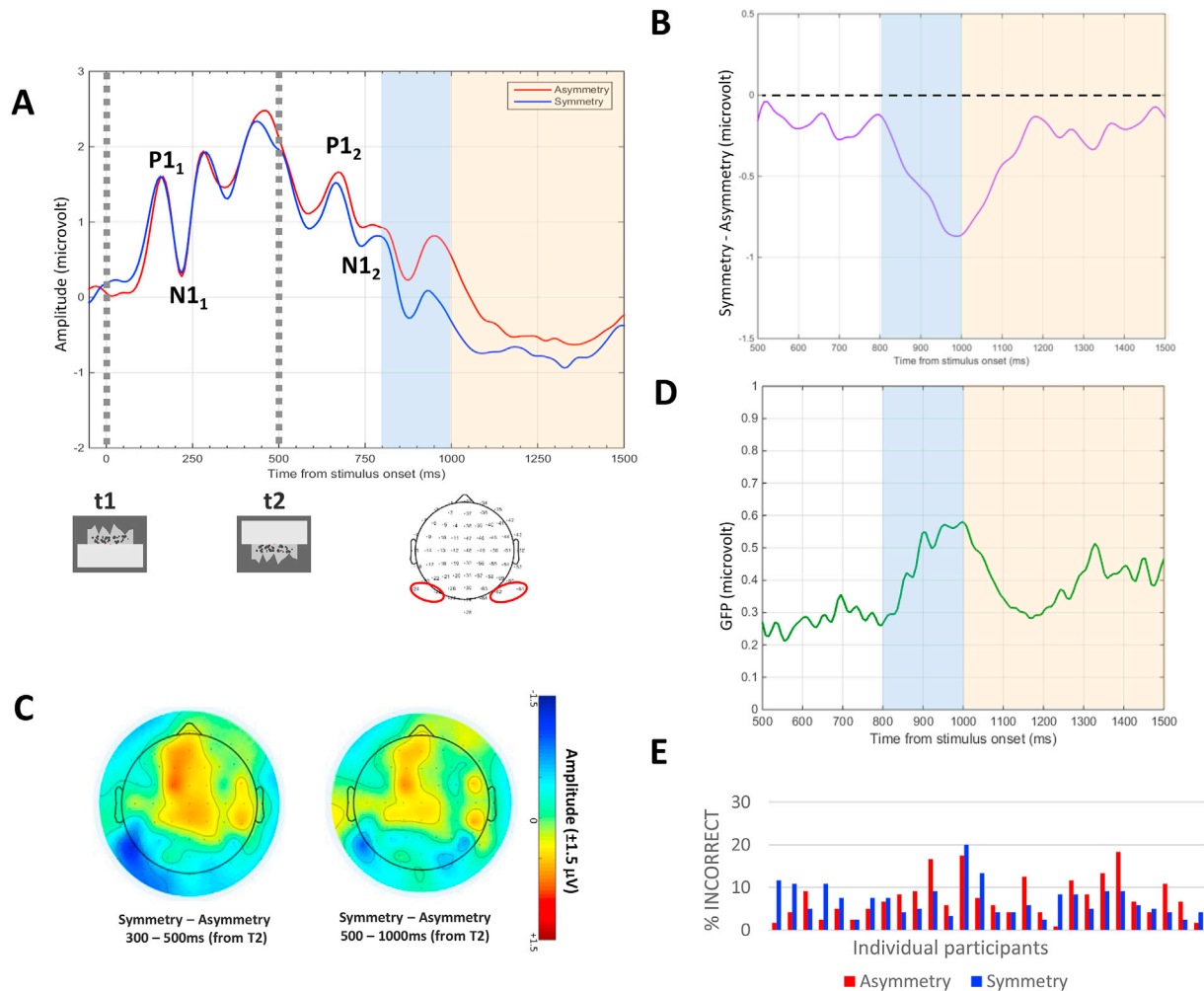

Fig. 5. *Experiment 2 Results* (A) Grand average ERP waves averaged across electrodes P9 PO7 P10 PO8. (B) Zoomed plot of the Grand average ERP shown as a difference wave (Symmetry – Asymmetry) from t_2. (C) Topographic difference maps (Symmetry – Asymmetry) from 300 to 500 ms and 500–1000 ms into t_2 (D) GFP plot in t_2. (E) Individual Percent Incorrect.

for the symmetry – asymmetry difference was performed on the log-transformed data. No significant difference between conditions was observed (t(27) = −0.01, p = 1). Fig. 5E reports the individual participant's percentage of incorrect responses in their original form. Note that ERPs analysis was performed only on trials where the correct decision was made.

3.1.2. ERPs

ERP results are shown in Fig. 5A–D. As expected, the results were like Experiment 1. Grand Average ERP data (electrodes P9 PO7; P10 PO8) from Experiment 2 were analysed with a 2 (Time-window) x2 (Hemisphere) x2 (Regularity) repeated measures ANOVA. The was a main effect of Regularity ($F_{(1,27)} = 8.2$, p = .008, partial $\eta^2 = 0.23$). The interactions between Time-window X Regularity ($F_{(1,27)} = 22.8$, p < .001, partial $\eta^2 = 0.46$) and the three-way interaction ($F_{(1,27)} = 12.0$, p = .002, partial $\eta^2 = 0.3$) were also significant (see Supplementary Material 1 for sequential Bonferroni control procedure on FWER). The interaction was further explored with simple main effects tests (Bonferroni corrected). In both time-windows, the symmetry – asymmetry difference was significant only in the left hemisphere. The difference was also stronger in the earlier window (M = −0.84, SE = 0.2; p < .001) than in the later one (M = −0.32, SE = 0.15; p = .04). This is clearly illustrated in the topographic maps in Fig. 5C. There was no other main effect or interaction (Fs < 2.5, ps > .1). Again, there was a GFP peak at approximately 980–1000 ms (Fig. 5D), which aligned with the peak of the different wave at observed from the posterior electrodes (Fig. 5B).

3.2. Discussion of experiment 2

Experiment 2 replicated both behavioural and ERP results of Experiment 1, using stimuli with a horizontal axis. In this case we observed a reduced, but significant, difference wave after the second half the shape was revealed. In line with Experiment 1, this peaked in the earlier time-window (i.e. 300 ms–500 ms from t_2). There is evidence of a slightly sustained response in this case, although only recorded in the left hemisphere. Leaving aside the time course, Experiment 2 replicated and extended the results of Experiment 1.

We observed that the symmetry-asymmetry response was lateralized to the left hemisphere. This result is inconsistent with other ERPs studies

showing that the symmetry response is generated by bilateral extrastriate visual areas bilaterally, and is often right lateralized (e.g. Makin et al., 2016, 2012a,b).

4. Experiment 3 (no occluder)

In Experiments 1 and 2 the dynamic display gave the impression of a whole object underneath a sliding rectangular occluder. An adaptive function attributed to symmetry is to signal objecthood (Baylis and Driver, 1995; Bertamini et al., 2002, 1997; Corballis and Roldan, 1974; Koning and Wagemans, 2009b; Makin et al., 2012a,b; Treder and van der Helm, 2007). We may expect that the reverse is also true: the brain computes the spatial relationship between the parts as a unit when they are first perceived to belong to the same object (Treder and van der Helm, 2007). In Experiment 3 there was no occluder and this gave the impression that the two halves were independent and complete shapes (Fig. 6). All other parameters were identical to Experiment 1.

4.1. Results

4.1.1. Behavioural

For the asymmetry condition mean percentage of incorrect responses was 6.5% (SE 0.81), and median was 5.4 (range 0–14); for the symmetry condition mean was 6.1% (SE 0.5 and median was 5.8 (range 0–11.7). Paired T-test for the symmetry – asymmetry difference was performed on the log-transformed data. No significant difference between conditions was observed (t(27) = −0.47, p = .6). Fig. 7E reports the individual participant's percentage of incorrect responses in their original form. Note that ERPs analysis was made only for trials where the correct decision was made.

4.1.2. ERPs

Results were largely like those of Experiments 1 and 2 (Fig. 7). Analysis was conducted on Grand Average ERPs (electrodes P9 PO7; P10 PO8). There was a main effect of Time-window ($F_{(1,27)} = 23.5$, p < .001, partial $\eta^2 = 0.46$), and Regularity ($F_{(1,27)} = 21.5$, p < .001, partial $\eta^2 = 0.41$). The interaction Time-window X Regularity ($F_{(1,27)} = 15.4$, p = .001, partial $\eta^2 = 0.36$) the three-way interaction ($F_{(1,27)} = 10.2$, p = .004, partial $\eta^2 = 0.32$) were significant (see Supplementary Material
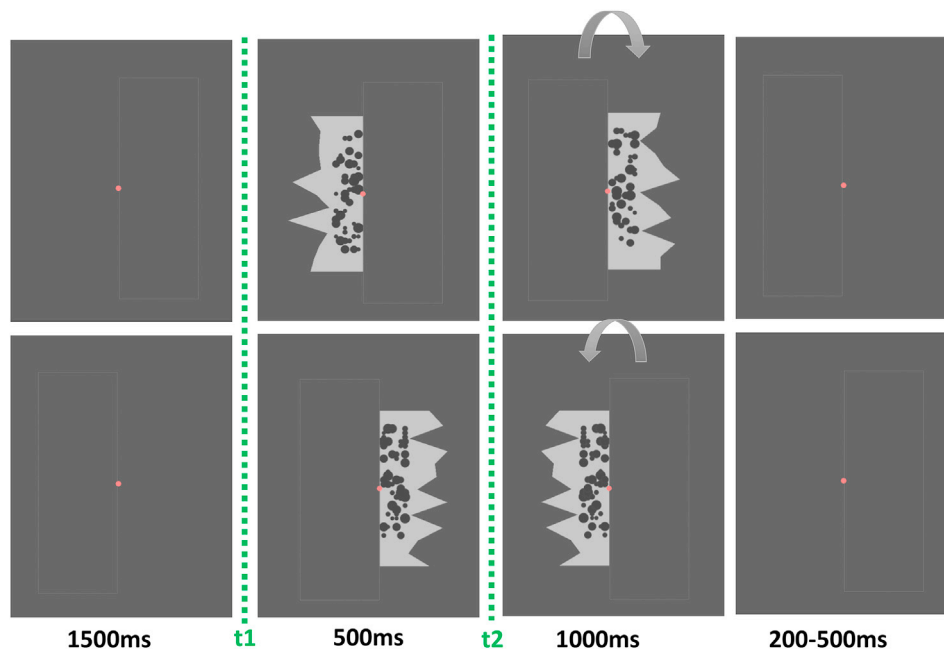

Fig. 6. Example of stimuli and experimental procedure in Experiment 3. These were identical to Experiment 1, but the occluder was absent. The dashed contour-line of the occluder has been added for illustrative purposes; it was not present in the experiment. In the figure both shapes are symmetric.
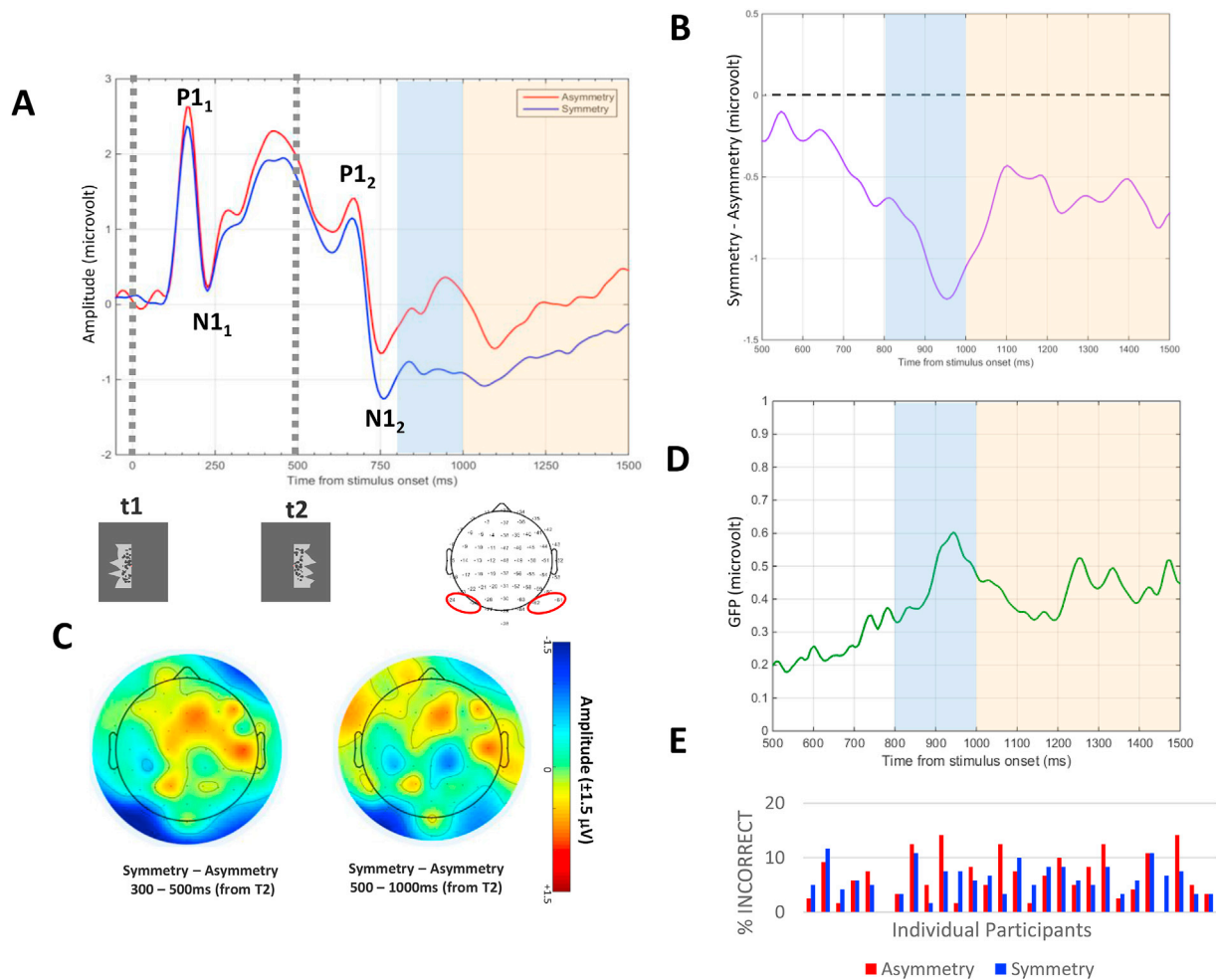
Fig. 7. *Experiment 3 Results* (A) Grand average ERP waves averaged across electrodes P9 PO7 P10 PO8. (B) Zoomed plot of the Grand average ERP shown as a difference wave (Symmetry – Asymmetry) from t2. (C) Topographic difference maps (Symmetry – Asymmetry) from 300 to 500 ms and 500–1000 ms into t2 (D) GFP plot in t2. (E) Individual Percent Incorrect.

1 for sequential Bonferroni control procedure on FWER). This was further explored with simple main effects tests (Bonferroni corrected). The symmetry – asymmetry amplitude difference was significant in both time-windows and both hemispheres, but stronger in the earlier time-window and in the left hemisphere (earlier time-window, left hemisphere: M = − 1.2, SE = 0.2, p < .001; right hemisphere: M = −0.7, SE = 0.2, p = .007; later time-window, left hemisphere: M = − 6, SE = 0.1, p < .001; right hemisphere: M = −0.4, SE = 0.2, p = .04). This is illustrated by the topographic maps in Fig. 7C. There was no other main effect or interaction (Fs < 0.3, ps > .6). The GFP analysis showed highest peak within the 300 ms - 500 ms time-window (Fig. 7D), reflecting the difference-ERP time-course and amplitude (Fig. 7B).

4.2. Discussion of experiment 3

Experiment 3 examined the role of the occluding rectangle. The results were similar to Experiments 1 and 2. Therefore, even without occlusion, the brain can detect the match between the two halves and integrate them to form a perceptual whole. This suggests an explicit occlusion is not necessary for integration.

There may be an important caveat: the rectangle in Experiments 1 and 2 provided a cue for occlusion, but functioned also as a mask. Ögmen and Herzog (2016), suggest that there are retinotopic and non-retinotopic components of sensory memory, which operate separately. Whilst the first is turned off by masking, the second is immune to it. If the observers can utilise the images stored in the *retinotopic Sensory Memory* the

integration of the visual transients is reinforced (Di Lollo et al., 1988). In Experiment 1 and 2 we recorded the integration of information stored at non-retinotopic level. In Experiment 3, a retinotopic imprint of the symmetrical image might be formed during the transition between t1 and t2. Although retinal afterimages and non-retinotopically stored images are separate phenomena (Di Lollo et al., 1988; Noory et al., 2015; Ögmen and Herzog, 2016), the synergistic effect of the two can reinforce temporal integration (Di Lollo et al., 1988). The combination of afterimage in the retinotopic store and persisted image in the non-retinotopic store could explain the more sustained SPN in Experiment 3.

This is in line also with recent results from Bertamini et al. (2019) who observed that brief presentations of symmetry trigger an SPN that persists at least a second after stimulus offset. The integration of independent parts into wholes will be further explored in Experiment 4.

5. Overall ERPs analysis from Experiment 1, 2 and 3.

Similar, but not identical, results were obtained from the three experiments. We therefore ran a powerful combined analysis with Experiment as a between participants factor to examine the commonalities and exceptions. We followed this with additional Mass Univariate and source localisation analysis to characterize the commonalities further.

5.1. Grand average ERPs: results and discussion

A mixed ANOVA was conducted with Experiment as between-subject

factor [3 (Experiment) X 2 (Time-window) X 2 (Hemisphere) X 2 (Regularity)]. There was a significant main effect of Time-window ($F_{(1,81)} = 54.8$, $p < .001$, partial $\eta^2 = 0.4$), and also a significant interaction Experiment X Time-window ($F_{(2,81)} = 6.9$, $p = .002$, partial $\eta^2 = 0.15$). The main effect of Regularity was significant ($F_{(1,81)} = 61.8$, $p < .001$, partial $\eta^2 = 0.3$), and this did not interact with Experiment ($p = .4$). There was a strong interaction Time-window X Regularity ($F_{(1,81)} = 80.5$, $p < .001$, partial $\eta^2 = 0.5$), and the interaction Time-window X Regularity X Experiment was significant too ($F_{(2,81)} = 6.1$, $p = .004$, partial $\eta^2 = 0.1$).

The interaction Time-Window X Hemisphere X Regularity was also significant ($F_{(1,81)} = 12.3$ $p = .001$, partial $\eta^2 = 0.1$). This interaction was further explored with simple effects tests (Bonferroni corrected; see also Supplementary Material 1 for sequential Bonferroni control procedure on FWER). The symmetry response was stronger in the first time-window and slightly stronger over the left hemisphere ($M = -1.0$, $SE = 0.1$, $p < .001$) than the right hemisphere ($M = -0.8$, $SE = 0.1$, $p < .001$). Similar lateralisation was observed in the second time-window (left: $M = -0.32$, $SE = 0.08$, $p < .001$; right: $M = -0.3$, $SE = 0.1$, $p = .009$). Interestingly, the four-factor interaction with Experiment was not significant ($F_{(2,81)} = 2.1$, $p = .1$, $\eta^2 = 0.05$).

This global analysis is relevant as it provides evidence that, despite some variations in the stimuli, all experiments showed consistent results: (i) a symmetry response was recorded 300 ms after t_2 (onset of second part of the shape); (ii) this response was stronger in the earlier time-window (i.e. 300 ms–500 ms from t_2), suggesting this is the timeframe when integration of the two parts happened; (iii) the symmetry response was generally significant in both hemispheres, although some tendency for left lateralisation was observed. These results are summarised graphically in Fig. 8, which shows the mean difference ERP amplitude symmetry – asymmetry in each experiment, hemisphere and time-window (see also Fig. 9C, which shows topographic maps of the symmetry activity in the two time-windows).

5.2. Mass-univariate analysis on single trials and source localisation analyses

An additional mass univariate analysis was performed on the ERP data from Experiment 1, 2 and 3 to assess the spatiotemporal development of the symmetry response after integration of the parts. This analysis tests differences between symmetry and asymmetry waves at all electrodes and points in time, dealing both with within-subject variance (i.e., single trial analyses) and between-subject variance. Fig. 9A shows that symmetry-related activity was concentrated 300 m - 500 ms after t_2 (i.e. onset of the second part of the shape). This confirms, again, that perceptual integration of the two halves of the shape took around 300 ms, and gave rise to a representation of object symmetry (see also Fig. 9B, which shows difference-ERPs from the selected individual electrodes with cluster-based correction). The application spatiotemporal clustering for multiple comparison corrections cancelled the significance over the

right hemisphere (right panel in Fig. 9A). The weaker right sided SPN did not survive such a conservative correction method.

The negativity observed over posterior electrodes in the 300 ms–500 ms time-window was associated with a positivity over frontal areas (electrodes Fz, AFz, F2, FCz), as it can be seen from the mass univariate analysis (Fig. 9A) and the topographic map (Fig. 9C). This is a typical topographic pattern of activation in ERP studies of symmetry (see Bertamini et al., 2018; Makin et al., 2016; Martinovic et al., 2018; Wright et al., 2018), which possibly reflects dipolar activity of occipital components (please see Supplementary Material 2, for ERP analyses and discussion of frontal electrodes' signal). Source localisation analysis on the 300 ms–500 ms topographic difference map showed that the extrastriate cortex generated the symmetry-integration process, with more pronounced activity over the left hemisphere (Fig. 9D). This confirmed that same cortical networks that respond to *symmetry in the image* (see Fig. 1C, Makin et al., 2012a,b) generate the representation of *symmetry in the object*, obtained through integration of transient parts.

Some residual activity was present over earlier visual areas, including V1 and V2 (central posterior regions in the longitudinal fissure). This was not predicted, as V1 and V2 do not usually distinguish between symmetrical and asymmetrical stimuli (e.g. Kohler et al., 2016; Sasaki et al., 2005). However, this early activation is not completely without precedent: Makin et al. (2016) observed a similar spread over V1 for highly salient regularities that strongly recruit extra-striate areas. Furthermore, the axis of reflection can be coded by orientation sensitive V1 cells based on top down inputs (Van Der Zwan et al., 1998). In this study the vertical axis might be particularly salient due to shift of the occluding edge. Top down inputs could potentially explain the apparent activation in V1.

Kohler et al. (2016) used a combination of fMRI and EEG and revealed rich representations of rotational symmetry present in retinotopically organised areas V3, hV4 and ventral occipital (VO1). Alp et al. (2018) used frequency tagging and found evidence of a progressive early visual cortex contribution to the global perception of symmetry. The widespread activation over early visual areas in our study may reflect the presence a recurrent feedback loops between higher and lower visual areas when progressively integrating retinal information that changes over time.

With respect to left hemispheric laterality, this might be associated to the novel task (i.e. spatiotemporal integration) introduced in this study. There is inconclusive evidence regarding hemispheric differences in symmetry perception. Some studies report a right-hemisphere superiority in symmetry perception (Bona et al., 2014; Makin et al., 2014; Prete et al., 2017; Wright et al., 2015). On the other hand, most evidence show bilateral activation. Wright et al. (2017) presented symmetric (and random) dot patterns in either the left or right side of the visual field. The left and right hemispheres were equally activated when the symmetry pattern was in their respective contralateral hemifield, and not modulated by what image was presented in the ipsilateral hemifield.

It is possible that the two hemispheres carry out specific aspects of symmetry processing when recruited simultaneously (e.g. to process a
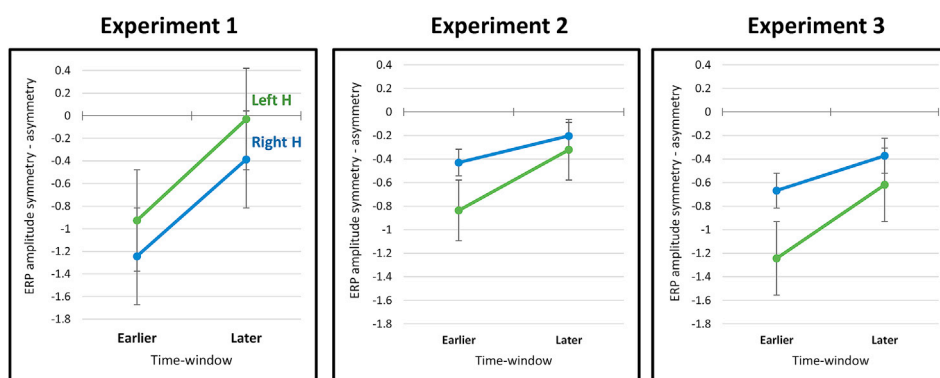

Fig. 8. Global analysis of Experiments 1–3. Line graph depicting the mean difference ERP amplitude symmetry – asymmetry for each experiment as a function of time-window and hemisphere. Earlier time-window is 300 ms–500 ms from t_2; Later time-window is 500 ms–1000 ms from t_2. Green lines indicate left hemisphere; Blue lines indicate right hemisphere. The value zero on the y axis indicates absence of a difference between symmetry and asymmetry, so all values below zero indicate greater ERP amplitude for symmetry compared to asymmetry. Error Bars = ±1 S.E.M.
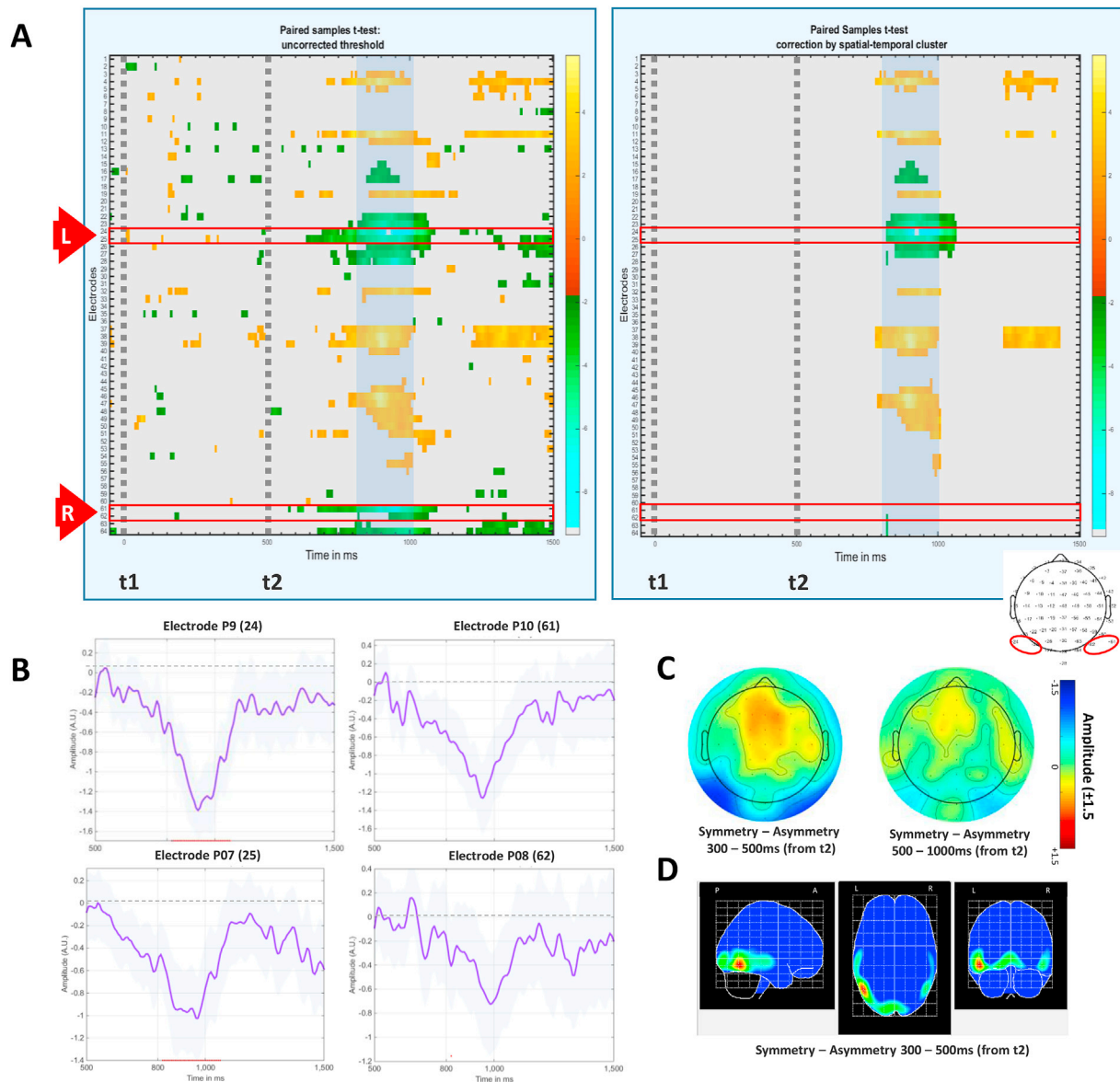
Fig. 9. Mass univariate and Source Localisation analysis on data from Experiment 1, 2 and 3 (N 84). (**A**) Mass-Univariate Analysis. Colour scale shows t scores from paired *t*-test (Symmetry vs. Asymmetry) both uncorrected for multiple comparisons (left) and corrected by spatio-temporal cluster-based computational methods (right). Negative t scores (symmetry < asymmetry) are blue/green, positive t scores (symmetry > asymmetry) are orange/red. All tests where p > .05 appear grey. X axis shows time from stimulus onset (including a baseline of −50 ms); Y axis shows electrode number from the BioSemi 64 electrode montage. Red arrows indicate L = left and R = right electrode clusters. The grey dotted lines indicate t_1 (onset of first half) and t_2 (onset of second half). The time-window of interest (300 ms–500 ms from t_2) is highlighted by blue box; this represents the moment in which integration of the two halves is predicted to happen and give representation of symmetry in the brain. The clusters of electrodes of interest were selected (red outline boxes) around electrodes PO7 (P9, PO7, left) and PO8 (P10, PO8; right), as these are the electrodes associated with symmetry visual processing in previous works (Martinovic et al., 2018; Bertamini et al., 2018). Surprisingly, activity over the right region was not significant when cluster-based correction was applied. (**B**) Paired Samples *t*-test waves (from 500 ms to end of epoch) from the selected individual electrodes with correction by spatial-temporal cluster (shaded blue area: 95% confidence intervals the; red dots below: significant difference from zero). (**C**) Topographic difference maps (Symmetry – Asymmetry) for the time-windows 300–500 ms (left) and 500–1000 ms (right) (from t_2). (**D**) Estimated cortical sources obtained with LORETA source localisation analysis. Data from the Grand-average difference topoplot shown in C (300 ms-500 ms from t_2) was used, and the estimated location of the generators is shown from three sections.

centrally presented symmetric pattern). For example, integrating spatial and temporal information recruits networks in the left inferior parietal cortex (Assmus et al., 2005). In our results, attention to spatiotemporal integration might have enhanced the responsiveness of the left lateralized symmetry-network. This is necessarily a post-hoc interpretation of these observations. A separate study should be specifically designed to explore hemispheric differences in the case of temporal integration of symmetry. We acknowledge that our source localisation procedure was not as sophisticated as those used in other recent studies (e.g. Kohler et al., 2016, 2018). The cortical sources estimated here are approximate,

and again require replication.

Finally, the results from the mass univariate and source localisation analyses justify our a priori choice of electrodes (P9, PO7; P10 and PO8), as they show clear posterior activity generated in the extra-striate cortex. This is consistent with the high levels of symmetry-related activity observed at electrodes PO7 (left) and PO8 (right) in previous studies (Bertamini et al., 2018; Makin et al., 2016; Martinovic et al., 2018; Wright et al., 2018). Moreover, a recent study using mass-univariate analysis found greatest symmetry-related activation in two lateralized clusters around electrodes PO7 and PO8 (Martinovic et al., 2018).

6. Experiment 4 (two halves)

In Experiments 1, 2 and 3 every time participants judged whether one half (presented a t_1) matched a second half (presented at t_2) there was an ERP response to the symmetry of the whole configuration. Perhaps the process of mapping one side with the other is the critical factor, even when these sides are presented sequentially and do not belong to the same object. In other words, *perception* of a whole object may not be necessary. Experiment 4 investigated this issue. We created a situation where the two halves were presented exactly as in Experiment 1. The key difference is that in this study the occluding rectangle was replaced by a second randomly constructed half, making a whole asymmetrical object. Therefore, the stimuli were always asymmetrical whole shapes and there was no occluder. Integration of the two symmetric halves was made within complete asymmetric shapes. By design, the right (or left) half in the first presentation could mirror reflect the left (or right) half in the second presentation (see Fig. 10A). A dark-grey line running down the centre of the screen separated the shapes in two halves. Participants were asked to attend to one half of the first shape (indicated by a small pink arrow above the stimulus) and match it with the opposite half of the second shape. They had to recognise whether the two parts matched and formed a symmetric or an asymmetric shape.

6.1. Results

For asymmetry condition, mean percentage incorrect was 12.1% (SE 1.2)and median was 10.8 (range 3.3–26.7); for symmetry mean was 14.2% (SE 1.7) and median was 12.1 (3.3–33.3). Paired T-test for the symmetry – asymmetry difference was performed on the log-transformed data. No significant difference between conditions was observed ($t(27) = -1.1$, $p = .3$). Fig. 10D reports the individual participant's percentage of incorrect responses in their original form.

ERPs analysis was performed only on trials where the correct decision was made. Fig. 10B and C suggest minimal ERP differences between symmetry and asymmetry conditions. The Time-window X Hemisphere X Regularity ANOVA did not reveal any significant effects ($Fs_{(1,27)} < 1.2$, $ps > .3$).

6.2. Discussion of experiment 4

This task was more difficult than previous experiments although accuracy remained well above chance (>70% of correct responses). Despite successful behavioural symmetry discrimination, no neural response to symmetry was recorded (note that we analysed only ERPs from trials where correct symmetry detection was made). This is the first case in which the ERP response is not indexed by performance in the regularity detection task, and it is important as it demonstrates that the SPN reflects perceptual mechanisms and not cognitive processes related to decisions about the presence of symmetry (Kohler et al., 2018; Palumbo et al., 2015).

Unlike Experiments 1, 2 and 3, there was no evidence of perceptual integration of the two halves. This is probably because the halves were automatically integrated with the visible, but task irrelevant other halves. This case resembles the *composite faces illusion*: if two faces are generated so that the top halves are identical whilst the bottom halves differ; people perceive the two top halves as being different (Rossion, 2013). In line with the Gestalt observation that the whole is different than the sum of its parts, the perception of one part of the *composite shape* is strongly influenced by the whole shape (Koffka, 1935; Pomerantz and Kubovy, 1986; Wertheimer, 1923).

If we consider the irrelevant-half acting as a mask, this result also provided another important piece of evidence. It is possible that when the mask is integrated with the target it interferes with the retention of the relevant information in the *non-retinotopic Sensory Memory (nrSM*
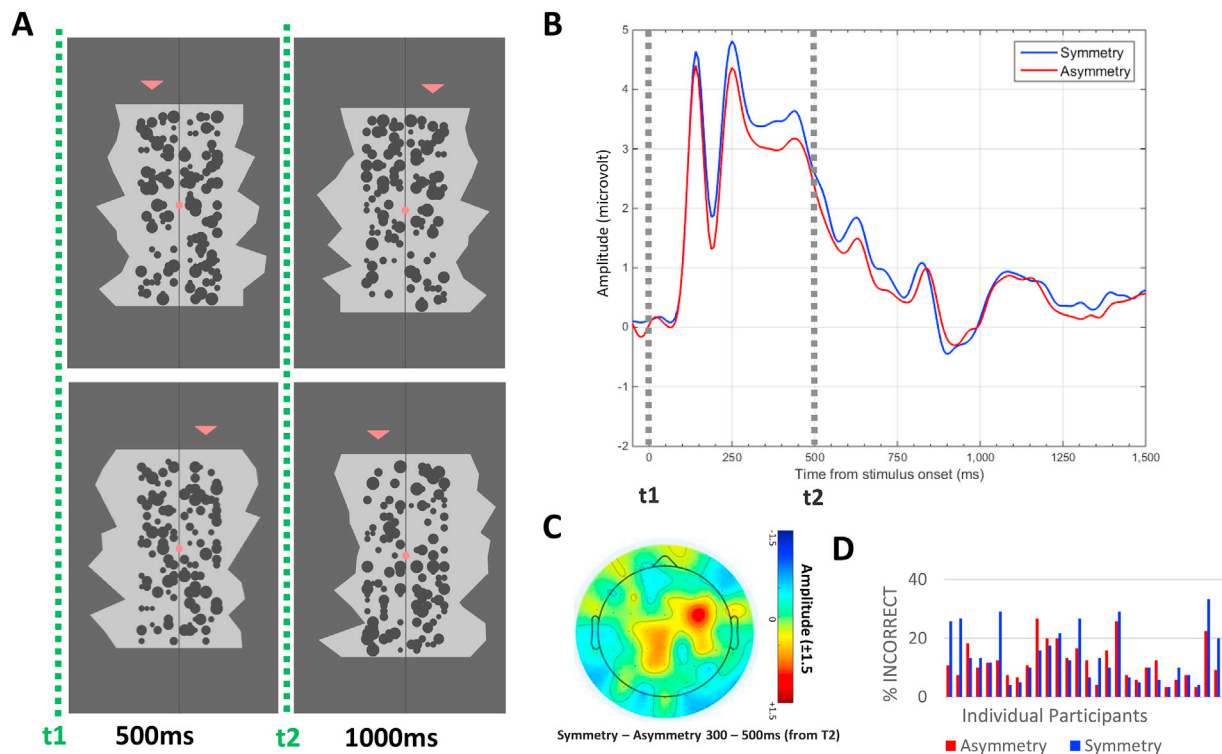

Fig. 10. *Method and Results of Experiment 4*. (A) Example stimuli: Two asymmetric shapes were presented one after the other. A dark line running down the screen divided the shape in two halves. A small arrow was presented over one of the two halves to indicate the half that should be attended. After 500 ms the arrow moved to the other side and simultaneously the shape changed. In 50% of trials the two halves indicated by the arrow were symmetrical to each other (top), in the other trials they were not (asymmetry, bottom). (B) Grand average ERP waves averaged across electrodes P9 PO7 P10 PO8. No symmetry – asymmetry response is observed at any point. (C) Topographic difference maps (Symmetry – Asymmetry in the time-window 300–500 ms. (D) Individual Percent Incorrect.

([Noory et al., 2015](#); [Öğmen and Herzog, 2016](#)). Thus, integration of visual transients into a holistic percept is prevented when the transient information is already perceptually claimed by different objects. Observers can still report the match, but this is done by a cognitive point by point comparison that is unlike perception of visual symmetry.

7. Experiment 5 (oddball)

We have established that the symmetry-network can compute the symmetry of parts presented at different points in time (unless they are perceived as belonging to different objects). This is an important computational process that goes beyond the symmetry in a given image. In the previous experiments participants were actively engaged symmetry computation – they had to find the correspondence or lack of correspondence between the halves. In this experiment, we investigated whether integration happens also when attention is directed away from the regularity, i.e. the match between the two halves. Participants performed an Oddball task on the same stimuli used in Experiment 1. They responded to the match/mismatch in colour between first and second half of the shape. In 20% of trials the second half was red rather than grey (as in the other 80% of trials). Participants had to pay attention to the shapes to perform the task, but not to the relationship between the shapes in the two intervals ([Fig. 11](#)).

7.1. Results

7.1.1. Behavioural

Participants made 0.8% incorrect responses in the non-oddball trials (SE 0.1) and 1.5% in the oddball trials (SE 0.4). Analysis was performed on log-transformed data, and no significant difference between conditions was observed ($t(26) = -1.1$, $p = .26$). ERPs analysis was performed only on trials where the correct decision was made.

7.1.2. ERPs

The Time-window X Hemisphere X Regularity ANOVA on non-oddball trials did not reveal any significant effect ($Fs_{(1,26)} < 0.7$, $ps > .3$) (See [Fig. 12](#)A and B). Oddball trials produced a significant P300 compared to non-oddball trial ($F_{(1, 26)} = 32.8$, $p < .001$, partial $\eta^2 = 0.6$), as expected ([Fig. 12](#)C and D). This was not affected by Regularity ($F_s < 0.7$, $p > .4$, partial $\eta^2 < 0.03$).

7.2. Discussion of experiment 5

Dynamic integration of symmetric parts does not happen automatically. There was no difference in the ERPs for symmetry and asymmetry conditions at any time. The large P300 recorded over centro-parietal electrodes confirmed that participants responded to the colour oddball, but they did not integrate symmetry from temporally separated halves. This is in line with previous studies that found that the *automatic* SPN was only elicited by information available in the retinal image ([Makin et al., 2015](#)). Similar to perspective normalisation, storing and integrating information non-retinotopically is a supplementary process. Without explicit task-requirements, the network does not spontaneously engage in it.

8. General discussion

There is a symmetry-sensitive network in extrastriate areas, including the Lateral Occipital Cortex ([Bertamini and Makin, 2014](#); [Bertamini et al., 2018](#); [Bona et al., 2014](#); [Chen et al., 2007](#); [Kohler et al., 2016](#); [Martinovic et al., 2018](#); [Sasaki et al., 2005](#); [Tyler et al., 2005](#); [Wright et al., 2018](#)). In ERP recordings, symmetry-related activity is indexed by a Sustained Posterior Negativity (SPN) over posterior electrodes starting approximately 300 ms from stimulus onset ([Bertamini et al., 2018](#); [Martinovic et al., 2018](#); [Wright et al., 2018](#)).

This study tested whether the symmetry-related ERP can be generated from integration of parts over time. In five experiments, two halves of a polygon was displayed one after the other. In some cases an occluder was perceived as covering and then uncovering the whole (Experiments 1 and 2). No reflection symmetry was ever displayed in the image at any point in time.

In Experiment 1 (vertical axis) and 2 (horizontal axis) the occluder was a white rectangle; in Experiment 3 the occluder was absent. The three experiments showed consistent results. In the first interval when only one part of the shape was displayed (t_1), no difference-ERP response was possible (or recorded). At this point in time, the participant had no way of knowing whether symmetry or asymmetry would be revealed in the second interval. When the occluder moved to the opposite side and revealed the second part of the shape (t_2), a SPN-like response was recorded. This was the case even in the absence of an occluder. This response indexed the integration of the old information in t_1 with the new information in t_2, showing that the symmetry network integrates information over time. Moreover, this response was stronger in the earlier part of the second time-window (i.e. 300 ms–500 ms from t_2). [Makin et al. (2016)](#) suggested that the SPN component may be split in two parts, in which the *early* component (peaking at 400 ms post onset) is a *pure* measure of stimulus regularity (see also [Wright et al., 2017](#)). The *sustained* response possibly reflects re-entrant processes or deployment of
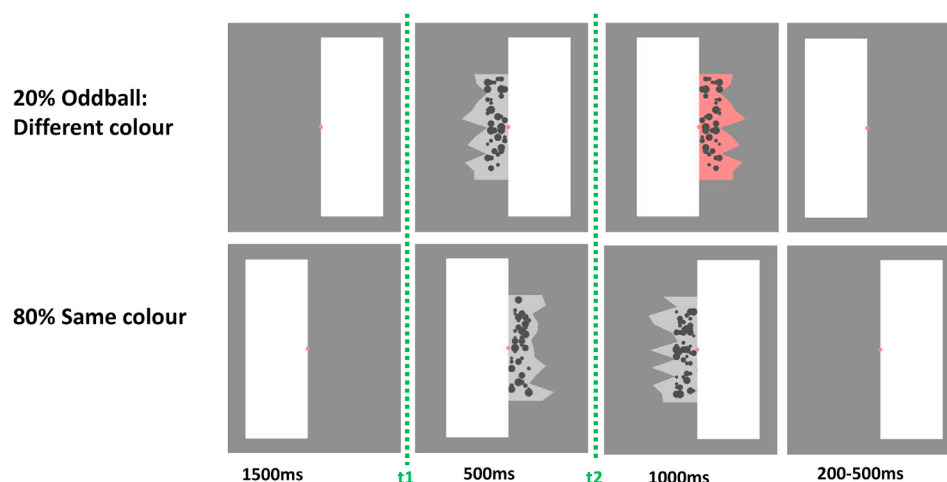

Fig. 11. Example of stimuli and experimental procedure in Experiment 5. The 80% of trials was identical to Experiment 1 (bottom). In the 20% of trials (oddball trials, at the top) the second half was coloured in red. Participants ignored the symmetry/asymmetry relationship between the two parts of the shape and were asked to report whether the colour of the second half was same or different from the first one.
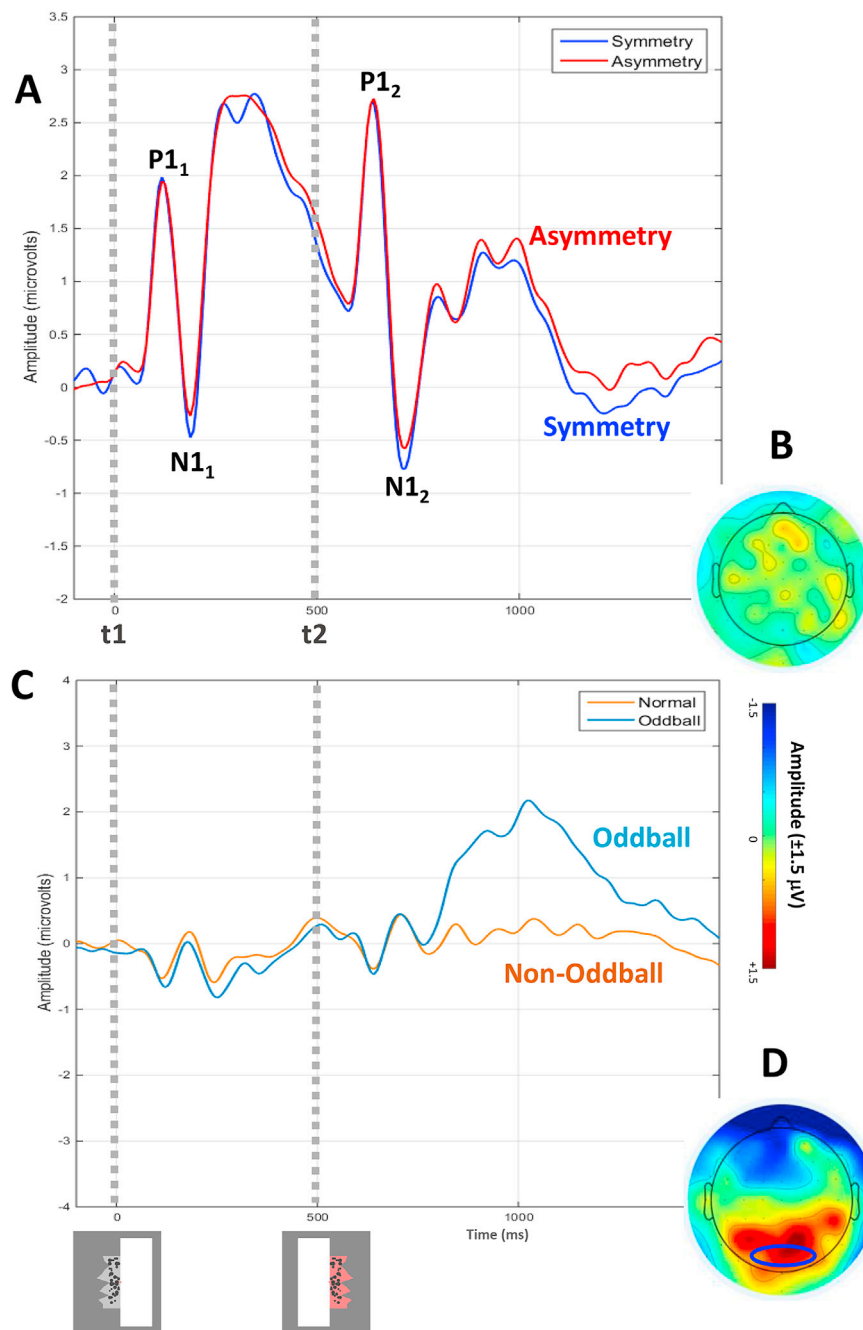
Fig. 12. (A) Grand average ERP waves averaged across electrodes P9 PO7 P10 PO8.No symmetry – asymmetry response is observed at any point. (B) Topographic difference maps (Symmetry – Asymmetry) showing the response to symmetry in the time-window 300–500 ms from t_2. (C) Grand average ERP from electrodes P1 Pz P2, showing the parietal P300 (D) Topographic difference maps showing the parietal P300 component (oval shows electrodes P1, Pz and P2).

spatial attention. Finally, the holistic representation of *symmetry in the object* was generated by same extrastriate cortical sources as those responding to *symmetry in the image* (Bertamini et al., 2018), although some tendency for left lateralisation was observed in this case (possibly due to the type of task).

We have seen a neural response to visual symmetry in the case of integration of parts over time. This confirms that the symmetry-sensitive areas can operate beyond local correlations in retinotopic coordinates. This is a striking evidence of the tuning of the visual system to symmetry in dynamic environments, when symmetrical objects rarely project perfectly symmetrical images on the retina in a single fixation.

The notion that the visual system retains briefly-viewed object

fragments in a *non-retinotopic space* so that they can be integrated with new information has been discussed in relation to other paradigms (Öğmen and Herzog, 2010, 2016; Palmer et al., 2006; Scharnowski et al., 2007). Importantly, global shape representation converges in LOC, either through direct processing of full image or spatiotemporal integration of parts, suggesting that this area may be the mediator of such temporal-integration processes (Orlov and Zohary, 2018). Moreover, behavioural evidence shows that the visual system can achieve global representations of symmetry through dynamic integration of consecutive brief presentations of symmetry patterns (Niimi et al., 2005, 2008; Sharman and Gheorghiu, 2017, 2018; Sharman et al., 2018; Tyler et al., 1995). Our results are thus timely and perfectly fit within this literature.

Here we further demonstrate the dynamic and integrative capacity of the extra-striate cortex, by showing that property-specific networks (i.e. symmetry-network) can achieve global representation of the property (i.e. symmetry) through spatiotemporal integration of parts.

Is it necessary to have a strong visual impression of a single, symmetrical object behind a moving occluder to generate an SPN at t_2? Experiment 3 did not support this hypothesis. The integration of the two halves (displayed as independent stimuli) still generated an SPN like component at t_2, even though there was no visible occluder to imply the presence of another, hidden part. However, this manipulation was not conclusive, and we cannot rule out either some role for afterimages or even perceived occlusion (despite no occluder was displayed). Experiment 4 allowed to test whether integrating parts from unrelated objects is a *sufficient* condition to elicit symmetry representation in the brain. The occluder had the same perceptual properties as the target stimulus (i.e. it was a second half of a different shape). This gave the percept of two unrelated asymmetric shapes presented in succession. Participants had to segregate the target-halves from the task-irrelevant asymmetrical whole shapes displayed in the image. We did not observe any ERP-difference between symmetry and asymmetry in Experiment 4. Participants could perform the task with >70% accuracy, so active comparison was still possible, but what was lacking was a percept of a symmetrical whole. This is evidence that the asymmetrical wholes dominated the percept both at t_1 and at t_2.

Finally, let us consider the results of Experiment 5. Here, the occluder was the same as in Experiment 1 and 2, but the task was to respond to an oddball (i.e. different colour of the second shape) and therefore there was no task involving symmetry discrimination. Directing participants' attention away from symmetry, depleted symmetry-related ERP after t_2. This result is in line with a previous study in which no response was recorded for distorted regularities in slanted perspectives (Makin et al., 2015). Processes like perspective normalisation (Keefe et al., 2018; Makin et al., 2015) and spatiotemporal integration are supplementary and they would waste neural resources if undertaken unnecessarily. It seems that the system engages in the extraction of object-based information only when this is task relevant. In contrast, image symmetry is extracted automatically and independently of task.

9. Conclusion

The human brain can store information provided at different points in time and integrate it to produce a holistic representation of the object. When this synthetic whole object is symmetrical, its representation generates the same neural response as a completely visible symmetrical object. In this study, we showed for the first time that the extrastriate symmetry network can perform spatiotemporal integration of symmetry as a property of the object, and the output of this computation has similar latency and topography to the response to symmetry in the retinal image. This process involves the recruitment of neural resources, and only occurs when attention is directed towards symmetry. However, it is not the case that every time that an observer can detect a match between shapes then there is a corresponding neural response. If the parts that must be integrated over time are already integrated into other asymmetrical objects, the neural symmetry response is absent. These findings improve our understanding of spatiotemporal integration processes as well as symmetry perception processes.

10. General methods

10.1. Participants

140 participants took part in the study (mean age 22.3 ($\pm$5), males 50, left handed 17), divided into groups of 28 participants for each experiment. One participant was not included in the analysis of Experiment 4, as responses incorrect were >45%. Participants had normal or corrected-to-normal vision. Some received either course credit or

financial reimbursement upon completion of the study. The study was approved by the University Ethics Committee and conducted in accordance with the Declaration of Helsinki (revised 2008).

10.2. EEG apparatus

EEG activity was recorded using a BioSemi (Amsterdam, The Netherlands) Active-Two amplifier in an electrically shielded and darkened room. EEG data was sampled continuously at 512 Hz from 64 scalp electrodes embedded in an elasticised cap arranged according to the standard international 10–20 system. Common Mode Sense (CMS) and Driven Right Leg (DRL) electrodes served as reference and ground. The same apparatus was used in Makin et al. (2012a,b) and other ERP-symmetry studies from our lab.

To detect blinks and eye movements, vertical bipolar electrodes (VEOG) were positioned above and below the right eye. Horizontal bipolar electrodes (HEOG) electrodes were positioned on the outer canthi of both eyes. Stimuli and experiment were programmed using the PsychoPy software (Peirce, 2007) and presented on a CRT monitor (1280 $\times$ 1024; 60 Hz, Mitsubishi; Tokyo, Japan). Participants were positioned 140 cm from the monitor with their head stabilized in a chin rest.

10.3. Stimuli

Stimuli consisted of unfamiliar polygon shapes (light grey colour (RGB [0.5, 0.5, 0.5], luminance 102.5 cd/m^2)) containing a dot pattern (dark grey colour (RGB [-0.5, −0.5, −0.5], luminance 10.5 cd/m^2)). The occluder was a light grey vertical bar (RGB [0.8, 0.8, 0.8], luminance 157.5 cd/m^2). These were presented on a grey background (RGB [-0.3, −0.3, −0.3], luminance 20.0 cd/m^2) (RGB colour space is expressed as deviations from grey ranging between −1 and 1; Peirce, 2007). All shapes were generated afresh on each trial and were all different from each other. No participant thus ever saw the same pattern twice.

For the generation of the polygon, one half was generated first. The other half was either mirrored (symmetry reflection condition) across the midline or a new polygon with same size and vertices (asymmetry condition) was generated. The half polygon was created by drawing one of the vertical contours with a random-walk algorithm. The contour was at a horizontal distance from fixation of approx. 2.4 ($\pm$0.8) degrees of visual angle and had 12 inward and outward turns with maximum and minimum displacement from the reference line of approx. $\pm$ 0.8 deg. These turns were equally spaced by approx. 0.7 deg on the Y-axis. The polygon height was approx. 7.2 deg. Top and bottom vertices were united with straight lines to form a closed polygon (resulting in one half of the stimulus shape). The dot pattern drawn inside each polygon (half of stimulus shape) was formed by approximately 40 dots (mean number of dots = 41.2, SD = 4.2). Dots radius varied randomly between 0.08 and 0.24 deg. Dots were placed in random positions within a matrix of 119 cells and confined within an area of 1.6 $\times$ 3 deg.

The occluder consisted on a rectangle of approx. size 6.1 $\times$ 12.3 deg. One vertical side of the occluder was aligned to the central midline to give the impression of covering exactly half of the stimulus shape.

Please note that throughout the manuscript we have used a terminology that reflects the natural way of describing the information in the stimuli, but it should be clear that the (dynamic) occlusion is a percept. A more objective, but less natural, terminology would be to say that we present an irregular polygon next to a rectangle in one interval. In the second interval, a rectangle is present at the location of the polygon, and a second irregular polygon is shown where the rectangle was before. In half of the trials the two polygons were one the reflection of the other, and in the other half the two polygons were unrelated to each other.

Stimuli variations in the different experiments

In Experiment 2 the exact same parameters were used, with the

difference that all stimuli and occluder were flipped on the horizontal plane. In this way, the two stimulus halves were visible either on the lower or upper side of the horizontal midline. In Experiment 3 the occluder was absent; in this way the two stimulus halves appeared as independent objects, and not as a half-occluded whole shapes.

In Experiment 4 there was no occluder. Participants saw two asymmetric shapes one after the other. A vertical (dark-grey) line running down the centre of the screen was used to highlight the split of the asymmetric shape in two halves. A light red arrow was used to point the half-shape participants should attend. In the symmetry condition, the first and second attended shape's halves were reflection symmetric to each other, whilst the unattended halves were randomly generated. In the asymmetric condition, all four shape's halves were randomly generated.

In Experiment 5 the second half of the polygon could be either coloured in grey as the first one (80% of trials), or in red (oddball trials: 20%).

10.4. Procedure

Prior to the beginning of the experiment, participants completed a practice block. Its design matched that of the main experiment in order to give participants the opportunity to familiarise themselves with the task. In the practice block a response feedback was provided to help participants understanding the task; this was not present in the experimental block. The practice consisted of 32 trials, as (most) participants required many repetitions to be able to perform the task. The experiment consisted of a total of 240 trials (60 for each condition). Participants were required to maintain fixation during the whole trial and retain from blinking when stimuli were displayed. Breaks were provided during the experiment to allow participants to rest and break fixation.

Participants were asked to fixate centrally throughout the whole trial. A short interval (200–500 ms) with only the fixation dot on screen, was followed by the baseline period (1500 ms) in which the occluder was shown. The occluder could be either at the left or right side of the central fixation midline (counterbalanced across trials). After baseline, the stimulus appeared (t_0). Only half of the stimulus was visible on the side not occupied by the occluder. At this point, participants could not predict whether the stimulus was reflection or asymmetry. The first half remained visible for 500 ms (t_1). The occluder then shifted to the opposite side and the second half of the pattern was revealed. This remained on the screen for 1000 ms (t_2). Stimulus recognition was supposed to happen at this time-window. After the stimulus shape disappeared, the occluder remained on the screen for another random interval (200–500 ms). A response screen was then presented indicating what button to press to enter the response (i.e. "Symmetry Asymmetry" or "Asymmetry Symmetry", counterbalanced across trials). Participants entered a response, by pressing either 'A' or 'L' button of the computer keyboard with their left or right index fingers. They were explicitly informed that responses needed to be as accurate as possible, whilst response speed was not measured. This was intended to minimize motor responses during the stimulus presentation period.

Note that the choice of stimulus duration was arbitrary. We used a long t_2 duration in order to explore the behaviour of the sustained response to symmetry after the integration of parts (1000 ms is a standard SPN time-window; e.g. Makin et al., 2012a,b, 2016; Wright et al., 2018). For the purpose of this study, we wanted to make sure that the first half of the pattern was fully processed; we thus used a relatively long t_1 duration (500 ms). Similarly, we have intentionally chosen not to include any variable temporal delay between the two halves to assess a continuous integration of parts. We acknowledge that the time variable (for both presentation durations and temporal interval) may play a role in this temporal integration of parts. This investigation would require a separate set of new experiments.

Variations in the different experiments.

Procedure was the same in all experiments. In Experiment 4 the red arrow was presented before the stimulus onset (duration: 1500 ms), indicating the to-be-attended half, and remained after stimulus offset (duration: 200–500 ms). Duration of first and second stimuli on screen was same as in the other experiments. In the Oddball task (Experiment 5) in the 20% of trials the stimulus half that was shown second was coloured in red. There were 320 trials in total. 64 trials were *oddballs* in which the second half was coloured in red. The other 256 trials were same as Experiment 1. In this experiment regularity was task-irrelevant. Participants ignored the presence of reflection symmetry within the stimuli and were required to report whether the colour of the two halves was 'Same' or 'Different'.

10.5. EEG analysis

EEG data was processed using the EEGLAB toolbox in MATLAB (Delorme and Makeig, 2004). This processing was designed to be as similar as possible to previous EEG studies (e.g. Makin et al., 2012a,b; see also review Bertamini and Makin, 2014 for more studies applying similar criteria). Data was referenced to a scalp average, and down-sampled to 128 Hz. We then segmented the data into -1 to 2 s epochs. Independent Components Analysis (ICA) was then used to remove oculomotor and other gross artefacts. After ICA, trials where amplitude exceed $\pm 100\,\mu V$ at any electrode were excluded. Moreover, trials where participants entered incorrect response were excluded from the ERP analysis. Therefore we included only trials in which transient information was correctly integrated. For the ERP analysis, we chose a cluster of posterior electrodes (left hemisphere: P9, PO7; right hemisphere: P10, PO8). These electrodes best represent the topographical distribution of the SPN and are normally used in ERP studies on symmetry (e.g. Martinovic et al., 2018; Wright et al., 2018; Makin et al., 2012a,b). We were interested in testing the activation of the extrastriate symmetry network when transient information about symmetry is integrated. Therefore, the amplitude of the Symmetry – Asymmetry difference was recorded starting from 300 ms after onset of the second half ($t_1 = 500$ ms), which corresponds to the classic SPN latency.

For Experiment 4 (oddball task) we also analysed the component P300, a positive wave in parietal electrodes produced by rare oddball trials compared to higher frequency non-oddball trials from 300 ms onwards. We analysed this response from the cluster of electrodes P1 Pz and P2 (same as in Makin et al., 2013).

ICA and trials rejection. In Experiment 1 on average 11 (SD = 4) out of 64 independent components were removed from each participant (min = 5, max = 19). After the data cleaning process, the total number of trials included in the analysis was between 55.35 (SD = 3) and 56.4 (SD = 3) for each of the four sub-conditions. In Experiment 2 an average of 13 components (SD = 2.3) was removed (min = 10, max = 18). Total number of trials for each sub-condition was between 51.6 (SD = 4) and 52.7 (SD = 4). In Experiment 3 an average of 13 components (SD = 3.4) was removed (min = 9, max = 22). Total number of trials analysed for each sub-condition was between 51.9 (SD = 4.5) and 52.3 (SD = 4.5). In Experiment 4 number of ICA components rejected was 9.6 (SD = 3, min = 2, max = 15), and trials included for each sub-condition ranged between 44 (SD = 8) and 47 (SD = 5). In Experiment 5 an average of 15 components (SD = 2) was removed (min = 12, max = 19). Total number of normal trials analysed for both symmetry and asymmetry was 121 (SD = 8 and SD = 9 respectively); it was 30 (SD = 2) and 31 (SD = 2) for oddball trials.

The ERPs data were normally distributed in all experiments (Shapiro-Wilk tests p > .05), in line with other similar studies in which SPN data are typically normally distributed (e.g. Makin et al., 2016). These were analysed with both repeated measure and mixed ANOVAs (see results sessions for more details). The Greenhouse-Geisser test correction factor was used when the assumption of sphericity was violated (Mauchly's test). Behavioural accuracy data were not normally distributed (Shapiro-Wilk test p < .05) in some cases (Experiment 1, asymmetry condition; Experiment 2, both regularity conditions; Experiment 4, both regularity conditions).

10.6. Global Field Power (GFP)

Global Field Power (GFP) is the standard deviation of amplitude across the 64 electrodes at a particular time point. GFP reflects the colour-variation in a topographic map. The higher variation in amplitude across the electrodes, the higher the GFP. GFP takes all the electrodes into account, therefore it can be used as further evidence that results are not dependent on electrode choice. Figs. 3D, 5D and 7D show that highest GFP peak was recorded around 900 ms–1000 ms (i.e. 400 ms–500 ms from t_2) in all three experiments.

10.7. Low resolution electromagnetic tomography (LORETA)

Source localisation analysis of the difference symmetry - asymmetry waves, was conducted using low resolution electromagnetic tomography (LORETA, Pascual-Marqui et al., 1994). The analysis was conducted using the Neuronic Source Localizer software (Neuronic, Havana, Cuba).

10.8. Mass univariate analysis

Mass-univariate analysis was used to assess the spatiotemporal development of the symmetry response. The analysis was conducted by using the LIMO EEG toolbox (Pernet et al., 2011). This analysis deals both with within-subject variance (i.e., single trial analyses) and between-subject variance; data are analysed using a hierarchical general linear model where parameters are estimated for each subject at each time point and each electrode independently (1st level analyses). Estimated parameters from the first level analyses are then integrated across subjects (2nd level analysis). With this approach, we conducted a paired *t*-test (categorical variable: symmetry vs. asymmetry). Fig. 9A plots the t-tests at all timepoints and electrodes (collapsed across the three experiments). The left panel shows results without correction for multiple comparisons. The panel on the right shows results using spatiotemporal clustering for multiple comparisons correction. This method uses the distribution of bootstrap clusters defined simultaneously in space and time; an observed spatial-temporal cluster of t-values is statistically significant if the sum of t-values contained in the cluster is bigger than the threshold bootstrap cluster sum obtained under H0 (Pernet et al., 2011; Pernet et al., 2015). A criterion p value of .05 was used; all areas in grey in Fig. 9A correspond to p > .05.

Acknowledgments

Appendix A. Supplementary data

Supplementary data related to this article can be found at https://doi.org/10.1016/j.neuroimage.2019.03.007. Raw data and analyses and codes of the experiments are available in the data repository: Open Science Framework (OSF, https://osf.io/b6hej/)

References

Alp, N., Kohler, P.J., Kogo, N., Wagemans, J., Norcia, A.M., 2018. Measuring integration processes in visual symmetry with frequency-tagged EEG. Sci. Rep. 8 (1), 6969. https://doi.org/10.1038/s41598-018-24513-w.

Assmus, A., Marshall, J.C., Noth, J., Zilles, K., Fink, G.R., 2005. Difficulty of perceptual spatiotemporal integration modulates the neural activity of left inferior parietal cortex. Neuroscience 132 (4), 923–927. https://doi.org/10.1016/j.neuroscience.2005.01.047.

Baijal, S., Srinivasan, N., 2011. Emotional and hemispheric asymmetries in shifts of attention: an ERP study. Cognit. Emot. 25 (2), 280–294. https://doi.org/10.1080/02699931.2010.492719.

Barlow, H.B., Reeves, B.C., 1979. The versatility and absolute efficiency of detecting mirror symmetry in random dot displays. Vis. Res. 19 (7), 783–793. https://doi.org/10.1016/0042-6989(79)90154-8.

Baylis, G.C., Driver, J., 1995. Obligatory edge assignment in vision - the role of figure and part segmentation in symmetry detection. J. Exp. Psychol. Hum. Percept. Perform. 21 (6), 1323–1342. https://doi.org/10.1037/0096-1523.21.6.1323.

Bertamini, M., Friedenberg, J., Argyle, L., 2002. No within-object advantage for detection of rotation. Acta Psychol. 111 (1), 59–81. https://doi.org/10.1016/S0001-6918(02)00043-4.

Bertamini, M., Friedenberg, J.D., Kubovy, M., 1997. Detection of symmetry and perceptual organization: the way a lock-and-key process works. Acta Psychol. 95 (2), 119–140. https://doi.org/10.1016/S0001-6918(96)00038-8.

Bertamini, M., Makin, A.D.J., 2014. Brain activity in response to visual symmetry. Symmetry 6 (4), 975–996. https://doi.org/10.3390/sym6040975.

Bertamini, M., Rampone, G., Oulton, J., Tatlidil, K.S., Makin, A.D.J., 2019. Sustained response to symmetry in extrastriate areas after stimulus offset: an EEG study. Sci. Rep. https://doi.org/10.1038/s41598-019-40580-z.

Bertamini, M., Silvanto, J., Norcia, A.M., Makin, A.D.J., Wagemans, J., 2018. The neural basis of visual symmetry and its role in mid- and high-level visual processing. Ann. N. Y. Acad. Sci. 1426, 1–16. https://doi.org/10.1111/nyas.13667.

Bona, S., Cattaneo, Z., Silvanto, J., 2016. Investigating the causal role of rightOFA in holistic detection of mooney faces and objects: an fMRI-guided TMS study. Brain Stimulation 9 (4), 594–600. https://doi.org/10.1016/j.brs.2016.04.003.

Bona, S., Herbert, A., Toneatto, C., Silvanto, J., Cattaneo, Z., 2014. The causal role of the lateral occipital complex in visual mirror symmetry detection and grouping: an fMRI-guided TMS study. Cortex 51 (1), 46–55. https://doi.org/10.1016/j.cortex.2013.11.004.

Bruno, N., Bertamini, M., Domini, F., 1997. Amodal completion of partly occluded surfaces: is there a mosaic stage? J. Exp. Psychol. Hum. Percept. Perform. 23 (5), 1412–1426. https://doi.org/10.1037/0096-1523.23.5.1412.

Carmody, D.P., Nodine, C.F., Locher, P.J., 1977. Global detection of symmetry. Percept. Mot. Skills 45 (3 Pt 2), 1267–1273. https://doi.org/10.2466/pms.1977.45.3f.1267.

Cattaneo, Z., 2017. The neural basis of mirror symmetry detection: a review. J. Cogn. Psychol. 29 (3), 259–268. https://doi.org/10.1080/20445911.2016.1271804.

Cattaneo, Z., Bona, S., Bauer, C., Silvanto, J., Herbert, A., Vecchi, T., Merabet, L., 2014. Symmetry detection in visual impairment: behavioral evidence and neural correlates. Symmetry 6 (2), 427–443. https://doi.org/10.3390/sym6020427.

Chen, C.C., Kao, K.L.C., Tyler, C.W., 2007. Face configuration processing in the human brain: the role of symmetry. Cerebr. Cortex 17 (6), 1423–1432. https://doi.org/10.1093/cercor/bhl054.

Cohen, E., Zaidi, Q., 2010. Salience of mirror symmetry in natural patterns. J. Vis. 7 (9), 970–970. https://doi.org/10.1167/7.9.970.

Corballis, M.C., Roldan, C.E., 1974. On the perception of symmetrical and repeated patterns. Percept. Psychophys. 16 (1), 136–142. https://doi.org/10.3758/BF03203266.

Dakin, S.C., Hess, R.F., 1997. The spatial mechanisms mediating symmetry perception. Vis. Res. 37 (20), 2915–2930. https://doi.org/10.1016/S0042-6989(97)00031-X.

Dakin, S.C., Watt, R.J., 1994. Detection of bilateral symmetry using spatial filters. Spatial Vis. 8 (4), 393–413.

Delorme, A., Makeig, S., 2004. EEGLAB: an open source toolbox for analysis of single-trial EEG dynamics including independent component analysis. J. Neurosci. Methods 134 (1), 9–21.

Di Lollo, V., Clark, C.D., Hogben, J.H., 1988. Separating visible persistence from retinal afterimages. Percept. Psychophys. 44 (4), 363–368. https://doi.org/10.3758/BF03210418.

Friedenberg, J., Bertamini, M., 2000. Contour symmetry detection: the influence of axis orientation and number of objects. Acta Psychol. 105. https://doi.org/10.1016/S0001-6918(00)00051-2.

Herbert, A.M., Humphrey, G.K., 1996. Bilateral symmetry detection: testing a "callosal" hypothesis. Perception 25 (4), 463–480. https://doi.org/10.1068/p250463.

Höfel, L., Jacobsen, T., 2007. Electrophysiological indices of processing aesthetics: spontaneous or intentional processes? Int. J. Psychophysiol. 65 (1), 20–31. https://doi.org/10.1016/j.ijpsycho.2007.02.007.

Jacobsen, T., Höfel, L., 2003. Descriptive and evaluative judgment processes: behavioral and electrophysiological indices of processing symmetry and aesthetics. Cognit. Affect Behav. Neurosci. 3 (4), 289–299. https://doi.org/10.3758/CABN.3.4.289.

Jenkins, B., 1983. Component processes in the perception of bilaterally symmetric dot textures. Percept. Psychophys. 34 (5), 433–440. https://doi.org/10.3758/BF03203058.

Julesz, B., 1971. Foundations of Cyclopean Perception. University of Chicago Press, Oxford. https://doi.org/10.1097/OPX.0b013e318155ab62.

Kanisza, G., Gerbino, W., 1982. Amodal completion: seeing or thinking? In: Beck E, B. (Ed.), Organization and Representation in Perception. Lawrence Erlbaum, New Jersey, pp. 242–248.

Keefe, B.D., Gouws, A.D., Sheldon, A.A., Vernon, R.J.W., Lawrence, S.J.D., McKeefry, D.J., et al., 2018. Emergence of symmetry selectivity in the visual areas of the human brain: fMRI responses to symmetry presented in both frontoparallel and slanted planes. Hum. Brain Mapp. 39 (10), 3813–3826. https://doi.org/10.1002/hbm.24211.

Koffka, K., 1935. Principles of Gestalt Psychology, vol. 20. International library of psychology philosophy and scientific method. https://doi.org/10.1037/h0052629.

Kohler, P.J., Clarke, A., Yakovleva, A., Liu, Y., Norcia, A.M., 2016. Representation of maximally regular textures in human visual cortex. J. Neurosci. 36 (3), 714–729. https://doi.org/10.1523/JNEUROSCI.2962-15.2016.

Kohler, P.J., Cottereau, B.R., Norcia, A.M., 2018. Dynamics of perceptual decisions about symmetry in visual cortex. Neuroimage 167 (April 2017), 316–330. https://doi.org/10.1016/j.neuroimage.2017.11.051.

Koning, A., Wagemans, J., 2009a. Detection of symmetry and repetition in one and two objects: structures versus strategies. Exp. Psychol. 56 (1), 5–17. https://doi.org/10.10 27/1618-3169.56.1.5.

Koning, A., Wagemans, J., 2009b. Detection of symmetry and repetition in one and two objects: structures versus strategies. Exp. Psychol. 56 (1), 5–17. https://doi.org/10.10 27/1618-3169.56.1.5.

Kourtzi, Z., Kanwisher, N.G., 2001. Human lateral occipital complex representation of perceived object shape by the human lateral occipital complex. Science 293 (2001), 1506–1509. https://doi.org/10.1126/science.1061133.

Lerner, Y., Hendler, T., Malach, R., 2002. Object-completion effects in the human lateral occipital complex. Cerebr. Cortex 12 (2), 163–177. https://doi.org/10.1093/cercor /12.2.163.

Mach, E., 1886. The Analysis of Sensations and the Relation of the Physical to the Psychical. Dover, New York, NY.

Makin, A.D.J., Pecchinenda, A., Bertamini, M., 2012a. Grouping by closure influences subjective regularity and implicit preference. I-Perception 3 (8), 519–527. https://do i.org/10.1068/i0538.

Makin, A.D.J., Rampone, G., Bertamini, M., 2015. Conditions for view invariance in the neural response to visual symmetry. Psychophysiology 52 (4), 532–543. https ://doi.org/10.1111/psyp.12365.

Makin, A.D.J., Rampone, G., Pecchinenda, A., Bertamini, M., 2013. Electrophysiological responses to visuospatial regularity. Psychophysiology 50 (10) n/a-n/a. https ://doi.org/10.1111/psyp.12082.

Makin, A.D.J., Rampone, G., Wright, A., Martinovic, J., Bertamini, M., 2014. Visual symmetry in objects and gaps. J. Vis. 14 (3), 1–12. https://doi.org/10.1167/14.3.12.

Makin, A.D.J., Wilton, M., Pecchinenda, A., Bertamini, M., 2012b. Symmetry perception and affective responses : a combined EEG/EMG study. Neuropsychologia 50 (14), 3250–3261. https://doi.org/10.1016/j.neuropsychologia.2012.10.003.

Makin, A.D.J., Wright, D., Rampone, G., Palumbo, L., Guest, M., Sheehan, R., et al., 2016. An electrophysiological index of perceptual goodness. Cerebr. Cortex 26 (12), 4416–4434. https://doi.org/10.1093/cercor/bhw255.

Martinovic, J., Jennings, B.J., Makin, A.D.J., Bertamini, M., Angelescu, I., 2018. Symmetry perception for patterns defined by color and luminance. J. Vis. 18 (8), 4. https://doi.org/10.1167/18.8.4.

Michotte, A., Thines, G., Crabbé, G., 1964. Les complements amodaux des structures perceptives (Amodal completion of perceptual structures). Studia Psychologica. Publications Universitaires de Louvain.[GV].

Niimi, R., Watanabe, K., Yokosawa, K., 2005. The role of visible persistence for perception of visual bilateral symmetry. Jpn. Psychol. Res. 47 (4), 262–270. https://doi.org/10. 1111/j.1468-5884.2005.00295.x.

Niimi, R., Watanabe, K., Yokosawa, K., 2008. The dynamic-stimulus advantage of visual symmetry perception. Psychol. Res. 72 (5), 567–579. https://doi.org/10.1007/s00 426-008-0133-y.

Noory, B., Herzog, M.H., Ogmen, H., 2015. Retinotopy of visual masking and non-retinotopic perception during masking. Atten. Percept. Psychophys. 77 (4), 1263–1284. https://doi.org/10.3758/s13414-015-0844-2.

Norcia, A.M., Candy, T.R., Pettet, M.W., Vildavski, V.Y., Tyler, C.W., 2002. Temporal dynamics of the human response to symmetry symmetric pattern random pattern. J. Vis. 2 (2), 132–139. https://doi.org/10.1167/2.2.1.

O'Reilly, R.C., Wyatte, D., Herd, S., Mingus, B., Jilk, D.J., 2013. Recurrent processing during object recognition. Front. Psychol. 4 (APR), 1–14. https://doi.org/10.33 89/fpsyg.2013.00124.

Öğmen, H., Herzog, M.H., 2010. The geometry of visual perception: retinotopic and nonretinotopic representations in the human visual system. Proc. IEEE 98 (3), 479–492. In: https://doi.org/10.1109/JPROC.2009.2039028.

Öğmen, H., Herzog, M.H., 2016. A new conceptualization of human visual sensory-memory. Front. Psychol. 7 (JUN), 1–15. https://doi.org/10.3389/fpsyg.2016.00830.

Orlov, T., Zohary, E., 2018. Object representations in human visual cortex formed through temporal integration of dynamic partial-shape views. J. Neurosci. 38 (3), 659–678. https://doi.org/10.1523/JNEUROSCI.1318-17.2017.

Osorio, D., 1996. Symmetry detection by categorization of spatial phase, a model. Proc. Biol. Sci. 263 (1366), 105–110. https://doi.org/10.1098/rspb.1996.0017.

Palmer, E.M., Kellman, P.J., Shipley, T.F., 2006. A theory of dynamic occluded and illusory object perception. J. Exp. Psychol. Gen. 135 (4), 513–541. https://doi.org/ 10.1037/0096-3445.135.4.513.

Palumbo, L., Bertamini, M., Makin, A., 2015. Scaling of the extrastriate neural response to symmetry. Vis. Res. 117, 1–8. https://doi.org/10.1016/j.visres.2015.10.002.

Papousek, I., Schulter, G., 2006. Individual differences in functional asymmetries of the cortical hemispheres. Cognit. Brain Behav. X (2), 269–298.

Pascual-Marqui, R.D., Michel, C.M., Lehmann, D., 1994. Low resolution electromagnetic tomography: a new method for localizing electrical activity in the brain. Int. J. Psychophysiol. 18 (1), 49–65. https://doi.org/10.1016/0167-8760(84)90014-X.

Peirce, J.W., 2007. PsychoPy - psychophysics software in Python. J. Neurosci. Methods 162 (1–2), 8–13. https://doi.org/10.1016/j.jneumeth.2006.11.017.

Pernet, C.R., Chauveau, N., Gaspar, C., Rousselet, G.A., 2011. LIMO EEG: A Toolbox for Hierarchical Linear Modeling of Electroencephalographic Data. Computational Intelligence and Neuroscience, 2011. https://doi.org/10.1155/2011/831409.

Pernet, C.R., Latinus, M., Nichols, T.E., Rousselet, G.A., 2015. Cluster-based computational methods for mass univariate analyses of event-related brain potentials/fields: a simulation study. J. Neurosci. Methods 250, 85–93. https:// doi.org/10.1016/j.jneumeth.2014.08.003.

Poirier, F. J. a M., Wilson, H.R., 2010. A biologically plausible model of human shape symmetry perception. J. Vis. 10 (1), 9.1–9.16. https://doi.org/10.1167/10.1.9.

Pomerantz, J., Kubovy, M., 1986. Theoretical approaches to perceptual organization: simplicity and likelihood principles. In: Boff, K.R., Kaufman, L., Thomas, J.P. (Eds.), Handbook of Perception and Human Performance. Wiley, New York, pp. 36.1–36.46.

Prete, G., Fabri, M., Foschi, N., Tommasi, L., 2017. Asymmetry for symmetry: right-hemispheric superiority in bi-dimensional symmetry perception. Symmetry 9 (5), 1–13. https://doi.org/10.3390/sym9050076.

Rainville, S.J.M., Kingdom, F.A.A., 2000. The functional role of oriented spatial filters in the perception of mirror symmetry - psychophysics and modeling. Vis. Res. 40 (19), 2621–2644. https://doi.org/10.1016/S0042-6989(00)00110-3.

Rampone, G., Makin, A.A.D.J., Bertamini, M., 2014. Electrophysiological analysis of the affective congruence between pattern regularity and word valence. Neuropsychologia 58 (1), 107–117. https://doi.org/10.1016/j.neuropsychologia.2014.04.005.

Rampone, G., O'Sullivan, N., Bertamini, M., 2016. The role of visual eccentricity on preference for abstract symmetry. PLoS One 11 (4). https://doi.org/10.1371/journ al.pone.0154428.

Rauschenberger, R., Liu, T., Slotnick, S.D., Yantis, S., 2006. Temporally unfolding neural representation of pictorial occlusion. Psychol. Sci. 17 (4), 358–364. https://doi. org/10.1111/j.1467-9280.2006.01711.x.

Rossion, B., 2013. The composite face illusion: a whole window into our understanding of holistic face perception. Vis. Cognit. 21 (2), 139–253. https://doi.org/10.1080/1350 6285.2013.772929.

Saarinen, J., 1988. Detection of mirror symmetry in random patterns at different eccentricities. Vis. Res. 28 (6), 755–759.

Sasaki, Y., Vanduffel, W., Knutsen, T., Tyler, C., Tootell, R., 2005. Symmetry activates extrastriate visual cortex in human and nonhuman primates. Proc. Natl. Acad. Sci. U. S. A 102 (8), 3159–3163. https://doi.org/10.1073/pnas.0500319102.

Sawada, T., Pizlo, Z., 2008. Detection of skewed symmetry. J. Vis. 8 (5), 14.1–14.18. https://doi.org/10.1167/8.5.14.

Scharnowski, F., Hermens, F., Herzog, M.H., 2007. Bloch ' s law and the dynamics of feature fusion. Vis. Res. 47, 2444–2452. https://doi.org/10.1016/j.visres.2007.05.00 4.

Scognamillo, R., Rhodes, G., Morrone, C., Burr, D., 2003. A feature-based model of symmetry detection. Proc. Biol. Sci. 270 (1525), 1727–1733. https://doi.org/10. 1098/rspb.2003.2434.

Sharman, R.J., Gheorghiu, E., 2017. The role of motion and number of element locations in mirror symmetry perception. Sci. Rep. 7 (March), 45679. https://doi.org/ 10.1038/srep45679.

Sharman, R.J., Gheorghiu, E., 2018. Spatiotemporal and luminance contrast properties of symmetry perception. Symmetry 10 (6). https://doi.org/10.3390/sym10060220.

Sharman, R.J., Gregersen, S., Gheorghiu, E., 2018. Temporal dynamics of mirror-symmetry perception. J. Vis. 18 (5), 10. https://doi.org/10.1167/18.5.10.

Shulman, G.L., Pope, D.L.W., Astafiev, S.V., McAvoy, M.P., Snyder, A.Z., Corbetta, M., 2010. Right hemisphere dominance during spatial selective attention and target detection occurs outside the dorsal frontoparietal network. J. Neurosci.: Off. J. Soc. Neurosci. 30 (10), 3640–3651. https://doi.org/10.1523/JNEUROSCI.4085-09.2010.

Treder, M.S., 2010. Behind the looking-glass: a review on human symmetry perception. Symmetry 2 (3), 1510–1543. https://doi.org/10.3390/sym2031510.

Treder, M.S., van der Helm, P.A., 2007. Symmetry versus repetition in cyclopean vision: a microgenetic analysis. Vis. Res. 47 (23), 2956–2967. https://doi.org/10.1016/j.vis res.2007.07.018.

Tyler, C.W., Baseler, H. a., Kontsevich, L.L., Likova, L.T., Wade, A.R., Wandell, B.A., 2005. Predominantly extra-retinotopic cortical response to pattern symmetry. Neuroimage 24 (2), 306–314. https://doi.org/10.1016/j.neuroimage.2004.09.018.

Tyler, C.W., Hardage, L., Miller, R.T., 1995. Multiple mechanisms for the detection of mirror symmetry. Spatial Vis. 9 (1), 79–100. https://doi.org/10.1163/156856 895X00124.

van der Helm, P. a., 2014. Symmetry perception. In: The Oxford Handbook of Perceptual Organisation, pp. 1–23 (August). https://doi.org/10.1097/MPG.0b013e3 18054b0dd.

van der Helm, P. a, Leeuwenberg, E.L., 1996. Goodness of visual regularities: a nontransformational approach. Psychol. Rev. 103 (3), 429–456. https://doi.org/10. 1037/0033-295X.103.3.429.

Van Der Zwan, R., Leo, E., Joung, W., Latimer, C., Wenderoth, P., 1998. Evidence that both area V1 and extrastriate visual cortex contribute to symmetry perception. Curr. Biol. 8 (15), 889–892. https://doi.org/10.1016/S0960-9822(07)00353-3.

Wagemans, J., Van Gool, L., D'ydewalle, G., 1991. Detection of symmetry in tachistoscopically presented dot patterns: effects of multiple axes and skewing. Percept. Psychophys. 50 (5), 413–427. https://doi.org/10.3758/BF03205058.

Wagemans, J., Van Gool, L., Swinnen, V.V., Van Horebeek, J., 1993. Higher-order structure in regularity detection. Vis. Res. 33 (8), 1067–1088. https://doi.org/10.1016/0042-6989(93)90241-N.

Wertheimer, M., 1923. Laws of Organization in Perceptual Forms. Untersuchungen zur Lehre von der Gestalt II. In: Psycologische Forschung. A Source Book of Gestalt Psychology, (1923), pp. 71–88. https://doi.org/10.1007/BF00410640.

Wright, D., Makin, A., Bertamini, M., 2015. Right-lateralized alpha desynchronization during regularity discrimination: hemispheric specialization or directed spatial attention? Psychophysiology 52 (5), 638–647. https://doi.org/10.1111/psyp.12399.

Wright, D., Makin, A.D.J., Bertamini, M., 2017. Electrophysiological responses to symmetry presented in the left or in the right visual hemifield. Cortex 86, 93–108. https://doi.org/10.1016/j.cortex.2016.11.001.

Wright, D., Mitchell, C., Dering, B.R., Gheorghiu, E., 2018. Luminance-polarity distribution across the symmetry axis affects the electrophysiological response to symmetry. Neuroimage 173 (October 2017), 484–497. https://doi.org/10.1016/j. neuroimage.2018.02.008.

Wyatte, D., Curran, T., O'Reilly, R., 2012. The limits of feedforward vision: recurrent processing promotes robust object recognition when objects are degraded. J. Cogn. Neurosci. 24 (11), 2248–2261. https://doi.org/10.1162/jocn_a_00282.